Seasonal Variation of Total Column Formaldehyde, Nitrogen Dioxide, and Ozone Over Various Pandora Spectrometer Sites with a Comparison of OMI and Diurnally Varying DSCOVR-EPIC Satellite Data

Jay Herman[1,2] and Jianping Mao[2,3]

[1]GESTAR II University of Maryland Baltimore County, Baltimore, Maryland USA

1000 Hilltop Cir, Baltimore, MD 21250

[2]NASA Goddard Space Flight Center, 8800 Greenbelt Road, Greenbelt, MD 20771, USA

Correspondence: Jay Herman (herman@umbc.edu)

[3]College of Computer, Mathematical and Natural Sciences, University of Maryland, College Park, MD 20740, USA

31 **Abstract**

32 Observations of trace gases, O_3, HCHO, and NO_2, and their seasonal dependence can be observed using
33 satellite and ground-based data from the Ozone Monitoring Instrument (OMI) satellite and Pandora
34 ground-based instruments. Both operate with spectrometers that have similar characteristics in
35 wavelength range and spectral resolution that enable them to retrieve total column amounts of
36 formaldehyde (TCHCHO), and nitrogen dioxide (TCNO2), and total column ozone (TCO). The polar
37 orbiting OMI observes at 13:30 ± 0:25 local time plus an occasional second side-scan point 90 minutes
38 later at mid-latitudes. The ground-based Pandora spectrometer system observes the direct sun all day
39 with a temporal resolution of 2 minutes. At most sites, Pandora data show a strong seasonal
40 dependence for TCO and TCHCHO and less seasonal dependence for TCNO2. Use of a low pass filter
41 Lowess(3-months) can reveal the seasonal dependence of TCNO2 for both OMI and Pandora at mid-
42 latitude sites usually correlated with seasonal heating using natural gas or oil. Compared to Pandora,
43 OMI underestimates the amount of NO_2 air-pollution that occurs during most days, since the OMI
44 TCNO2 retrieval is around 13:30± 0:25 local time, which tends to occur near the frequent minimum of
45 the daily TCNO2 time series. Even when Pandora data are restricted to between 13:00 and 14:00 hours
46 local time OMI retrieves less TCNO2 than Pandora over urban sites because of OMI's large field of view.
47 The seasonal behavior of TCHCHO is mostly caused by the release of HCHO precursors from plant
48 growth and emissions from lakes that peak in the summer as observed by Pandora and OMI. Long-term
49 averages show that OMI TCHCHO usually has the same seasonal dependence but differs in magnitude
50 from the amount measured by Pandora and is frequently larger. Comparisons of OMI total column NO_2
51 and HCHO with Pandora daily time series show both agreement and disagreement at various sites and
52 days with Pandora frequently larger. For ozone, daily time dependent comparisons of OMI TCO with
53 those retrieved by Pandora show good agreement in most cases. Additional diurnal comparisons are
54 shown of Pandora TCO with hourly retrievals during a day from EPIC (Earth Polychromatic Imaging
55 Camera) spacecraft instrument orbiting the Earth-Sun Lagrange point L_1.

56 **1.0 Introduction**

57 Formaldehyde, HCHO, is ubiquitous in the atmosphere and as with other VOCs (Volatile Organic
58 Compounds) are derived from natural and anthropogenic sources, such as plants, animals, biomass
59 burning, fossil fuel combustion, and industrial processes (Zhang et al., 2019; Morfopoulos et al., 2021).
60 Formaldehyde is mainly produced from the oxidation of VOCs such as isoprene, methane, and
61 anthropogenic emissions (Wittrock, 2006). Formaldehyde can also be directly emitted from some
62 sources, such as vehicle exhaust, tobacco smoke, building materials, and wood burning affecting
63 pollution levels both indoors and outdoors. The majority of gaseous and atmospheric formaldehyde
64 derives from microbial and plant decomposition (Peng et al., 2022). HCHO concentrations in the first few
65 kilometers of the atmosphere vary depending on the location, time of day, season, and meteorological
66 conditions. Some of the factors that influence total atmospheric column amounts of HCHO are:

67 • **Solar radiation**: Formaldehyde is photolyzed by solar ultraviolet radiation (Nussbaumer et al., 2021)
68   and broken down into smaller molecules and radicals. The photolysis rate of formaldehyde depends
69   on the solar zenith angle, the cloud cover, and the atmospheric composition. Generally,
70   formaldehyde photolysis is faster in the summer and during midday.
71 • **Temperature**: The thermal decomposition rate of formaldehyde increases with temperature, which
72   means it is faster in warmer regions and seasons.
73 • **Humidity**: Formaldehyde reacts with water vapor in the atmosphere, forming formic acid and
74   hydroxyl radicals. The reaction rate of formaldehyde with water vapor depends on the relative

75   humidity, which varies with the temperature and the precipitation. Generally, formaldehyde
76   reaction with water vapor is faster in humid regions and seasons.

77

78 The largest sources of NO_2 are obtained from fossil fuel burning from various types of automobiles truck
79 emissions and power generation followed by industrial processes and oil and gas production (Van der A,
80 2008; Stavrakou et al. 2020). Additional sources are soils with natural vegetation, oceans, agriculture
81 with the use of nitrogen rich fertilizers, forest fires, and lightning. In populated areas requiring winter
82 heating, anthropogenic sources of lower tropospheric NO_2 are larger than natural sources. Nitrogen
83 oxides play a major role in atmospheric chemistry and the production and destruction of ozone in both
84 the troposphere and stratosphere. In the boundary layer high concentrations of both HCHO (Kim et al.,
85 2011) and NO_2 (Faustini et al., 2014) are health hazards for humans.

86

87 TCHCHO, TCNO2 and TCO in the atmosphere are typically measured by satellite and ground-based
88 instruments.

89 • Satellite: The Ozone Monitoring Instrument (OMI) is a satellite sensor launched in July 2004 that
90   measures HCHO, NO_2, O_3, and other atmospheric constituents from space (Levelt et a. 2018).
91   Detailed descriptions of the OMI instrument are given in Levelt et al. (2006) and Dobber et al.
92   (2006). Briefly, OMI is a side scanning spectrometer instrument (270 to 500 nm in steps of 0.5 nm)
93   with a nadir spatial resolution or 13 x 24 km^2. OMI data can be used to monitor their global
94   distribution and long-term trends, and to investigate the role of NO_2 and HCHO in atmospheric
95   chemistry and air quality (Lamsal et al., 2014; 2015; Boeke et al., 2011). For ozone, DSCOVR (Deep
96   Space Climate Observatory), located at the Earth-Sun gravitational balance Lagrange point L_1,
97   contains a filter-based instrument EPIC (Earth Polychromatic Imaging Camera) capable of obtaining
98   TCO once per hour (90 minutes in Northern hemisphere winter) simultaneously for the entire sunlit
99   globe as the Earth rotates (Herman et al., 2018) with nadir resolution of 18 x 18 km^2.
100 • Ground-based Spectrometer: The Pandora spectrometer system forms a worldwide network of over
101   150 currently working direct-sun observing instruments that match atmospheric observations with
102   known laboratory spectra of HCHO, NO_2, and O_3 to obtain the total vertical column above the
103   Pandora instrument every 2 minutes from multiple co-added spectra. Pandora uses a single-grating
104   spectrometer and a charge-coupled device (CCD) 2048 x 64-pixel detector to record the direct-sun
105   spectra in the ultraviolet and visible wavelength range, 280 – 525 nm with an oversampled 0.6 nm
106   spectral resolution. The retrieval algorithm is based on a spectral fitting technique to retrieve the
107   slant column densities of O_3, HCHO, NO_2 and other gases, and then convert them to vertical column
108   densities using geometric air mass factors appropriate for direct-sun observations. Pandora
109   spectrometers have been deployed in various field campaigns and locations to monitor the spatial
110   and temporal variability of TCHCHO and TCNO2 to validate and improve the satellite observations of
111   TCHCHO (Herman et al., 2009, Tzortziou et al., 2015, Spinei et al., 2018).

112

113 Previous validation studies of $TCNO_2$ and TCHCHO have been made with emphasis on the amount of bias
114 between ground-based and satellite retrievals of total column NO_2 and HCHO (Pinardi et al., 2020; de
115 Smedt et al., 2021) and references therein. Validation studies using Pandora measurements have shown
116 that OMI TCNO2 retrievals tend to underestimate the degree of NO_2 pollution, especially in urban areas
117 where the coarse OMI spatial resolution tends to reduce the spatially averaged amount (Celarier et a.,
118 2008; Lamsal et al., 2014; Judd et al., 2019; Zhao et al., 2019). In addition to the different field of view,
119 the agreement between OMI and Pandora depends strongly on determining the OMI effective air mass

120 factor for a wide variety of observing and solar zenith angles (Lorente et al., 2017), whereas Pandora
121 uses a simple geometric direct sun airmass factor (Herman et al., 2009, Eq 3). Studies of TCHCHO
122 involving Pandora prior to 2020 are probably not valid because of a problem with internal generation of
123 HCHO in the Pandora instrument (Spinei et al., 2021). More recent studies (Wang et al. 2022) obtain a
124 seasonal dependence of surface concentrations similar to the TCHCHO in this study. The largest sources
125 of error in TCHCHO retrievals are the determinations of the air mass factor for satellite observations and
126 the fact that ozone and formaldehyde have overlapping absorption spectra so that a small error in
127 ozone retrieval can affect the formaldehyde results. A comparison of direct-sun Pandora TCHCHO
128 retrievals with Geostationary Environment Monitoring Spectrometer GEMS shows a similar seasonal
129 dependence (Fu et al., 2025).

130

131 This study will examine the offsets and seasonal cycles of total column NO_2, HCHO, and O_3 seen by the
132 Pandora instruments by examining multi-year (2021 – 2024) time series for seasonal and daily behavior
133 at various sites and will compare with observations made from the OMI satellite overpass
134 measurements (based on OMI gridded 0.25^O x 0.25^O data) for the Pandora sites. Pandora ozone
135 measurements will be additionally compared to hourly data obtained from EPIC. All of the Pandora data
136 used in this study are after the upgrade of the instruments to eliminate internal sources of HCHO
137 (Spinei, et al., 2021). Part of this study (TCNO2 and TCO) is an extension of Herman et al. (2019) using
138 Pandora data (2012 – 2017) before the internal upgrade. A difference is that Pandora TCO is now
139 compared with hourly TCO retrieved by DSCOVR-EPIC. Table 1 shows a list of 30 Pandora sites used in
140 this study.

141

Table 1 List of 30 Pandora locations used in this study in order of appearance

	Pandora Number	Pandora location name	Lat (deg)	Long (deg)	Alt(m)
1	Pan 180 Fig.1,2	Bronx, New York USA	40.868	-73.878	31
2	Pan 64 Fig.3	New Haven, Connecticut USA	41.301	-72.903	4
3	Pan 190 Fig.4	Bangkok, Indonesia	13.785	100.540	6
4	Pan 182 Fig.5	Tel Aviv, Israel	32.113	34.806	8
5	Pan 159 Fig. 6	Wakkerstroom, South Africa	-27.349	30.144	18
6	Pan 20 Fig.7	Busan, Korea	50.798	4.358	107
7	Pan 145 Fig.10	Toronto-Scarborough, Canada	43.784	-79.187	14
8	Pan 134 Fig. 12	Bristol, Pa, USA	40.107	-74.882	10
9	Pan 204 Fig. 12	Boulder, Co USA	40.038	-105.242	161
10	Pan 106 Fig.12,A2	Innsbruck, Austria	47.264	11.385	616
11	Pan 117 Fig.12	Rome Italy	41.907	12.5158	75
12	Pan 193 Fig.12	Tsukuba, Japan	36.066	140.124	51
13	Pan 140 Fig.13,A2	Washington, DC USA	38.922	-77.012	6
14	Pan 166 Fig.7,A2	Philadelphia, Pa USA	39.992	-75.081	6
15	Pan 238 Fig.14	Granada	37.164	-3.605	7
16	Pan 240 Fig. 14	Thessaloniki, Greece	40.6336	22.9561	60
17	Pan 66 Fig.15	Huntsville Alabama USA	34.725	-86.646	22
18	Pan 156 Fig.15	Hampton, Virginia USA	37.020	-76.337	19
19	Pan 39 Figs.12,15	Dearborn, Michigan USA	42.307	-83.149	18
20	Pan 101 Fig.A1	Izania, Spain	28.309	-16.499	24
21	Pan 119 Fig.A1,A2	Athens, Greece	37.998	23.775	130
22	Pan 124 Fig.A1	Comodoro Rivadavia	-45.7833	-67.45	46
23	Pan 131 Fig. A1	Palau	7.3420	134.4722	23
24	Pan 135 Fig.A1,A2	CCNY Manhattan NY USA	40.815	-73.951	34
25	Pan 142 Fig.A1	Mexico City, Mexico	19.326	-99.176	2280

26	Pan 146 Fig.A1	Yokosuka, Japan	35.321	139.651	5
27	Pan 147 Fig.A1	Detroit, Mi USA	42.303	-83.107	178
28	Pan 150 Fig.A1,A2	Ulsan, Korea	35.575	129.190	38
29	Pan 154 Fig.A1	Salt Lake City Ut, USA	40.766	-75,081	1455
30	Pan 162 Fig.A1	Brussels, Belgium	50.798	4.358	107

142

2.0 Examples of Seasonal and Daily Variation of HCHO and NO$_2$

144 Worldwide Pandora total column data can be downloaded from the Austrian Pandonia project website
145 https://data.pandonia-global-network.org/. Of interest for this study are the Level-2 (L2) time series
146 ASCII files for direct-sun observations. For example, the Bronx New York City files for Pandora
147 instrument 180 for TCNO2 data are in Pandora180s1_BronxNY_L2_**rnvs3p1-8**.txt, TCHCHO in
148 Pandora180s1_BronxNY_L2_**rfus5p1-8**.txt, and TCO data in Pandora180s1_BronxNY_L2_**rout2p1-8**.txt
149 with the 9 bold characters identifying the file contents. This naming convention applies to all Pandora
150 sites.

151 The Pandora data are arranged in irregular columns that are identified in the metadata header for each
152 file. In the current version, column 1 contains the GMT date and time for each measurement and
153 column 39 contains measured column density in moles m^{-2} (multiply by 6.02214076x10^{23}/2.6867 x10^{20} =
154 2241.4638 to convert to DU where 1 DU = 2.6867 x 10^{20} molecules m^{-2}). Pandora data also contain
155 measurements of water vapor, and SO$_2$ total column amounts in different files.

156 The original OMI data has a resolution of 13 x 24 km^2 at the center of the OMI side-to-side scan. The
157 overpass OMI data is based on the latest gridded version with 0.25^O x 0.25^O pixel resolution
158 (midlatitudes approximately 30 x 30 km^2). The closest OMI pixel to each Pandora site within 50 km
159 is used for time-matched comparisons. Long time series use all available Pandora data between
160 07:00 and 17:00 filtered for data quality (values with large RMS errors and with negative values are
161 removed). Diurnal comparisons with OMI on specified days use Pandora minute-by-minute data
162 that are nearly continuous suggesting that Pandora is observing the direct sun under clear-sky
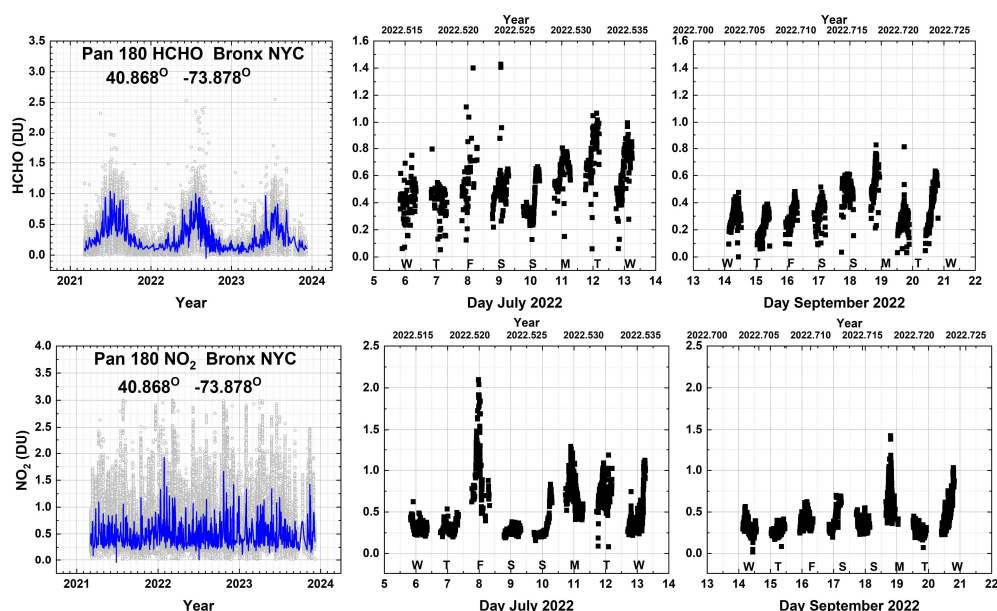163 conditions. Clouds cause some scatter in consecutive data points.

Fig. 01 Seasonal and daily behavior of HCHO and NO_2 from Pan 180 located in the Bronx, NYC at 40.868^{O}N, -73.878^{O}W. The blue lines are a Lowess(0.033) fit to the data (light grey), which is approximately a 1-month local least-squares average. The Local principal investigator for Pan 180 is Dr. Luke Valin.

164   Figure 1 shows the seasonal and daily variation of total column HCHO (TCHCHO) and NO_2 (TCNO2) in
165   Bronx, New York. The daily data for 1 week in July and September shows the range of values for both
166   weekdays and weekends. When all the Bronx TCHCHO data are plotted as an aggregate for 3 years, there
167   is a strong seasonal pattern with a maximum in July and a minimum near the end of December. The
168   summer seasonal dependence of TCHCO is consistent with the surface HCHO values observed by the
169   ground-based Air-Quality System AQS (Wang et al., 2022). For TCNO2, there is a weaker seasonal
170   pattern as shown in the Lowess(0.033) fit to the data (Cleveland, 1979; Cleveland and Devlin, 1988) with
171   moderate maxima in January-February, since the sources of NO_2 are largely from the nearly constant
172   flow of cars and trucks. The parameter 0.033 is the fraction of the time-series data included in the local
173   least squares estimate, or about 1 month for Pan 180.

174

175   Figure 2 shows the daily average of Pandora data obtained from diurnal variation of TCHCHO and TCNO$_2$
176   from 09:00 to 15:00 local standard time (GMT − 5). The primary emission sources of atmospheric HCHO
177   include direct emissions of HCHO precursors from vegetation and lakes, primarily through the release of
178   biogenic volatile organic compounds such as isoprene and terpenes from vegetation, the soil, biomass
179   burning, and decaying plant and animal matter. This is consistent with the Bronx location that is
180   adjacent to a large, vegetated park with a small lake near Fordham University. The same TCHCHO
181   seasonal dependence and magnitude occurs when the Pandora sampling is restricted to 13:00 to 14:00
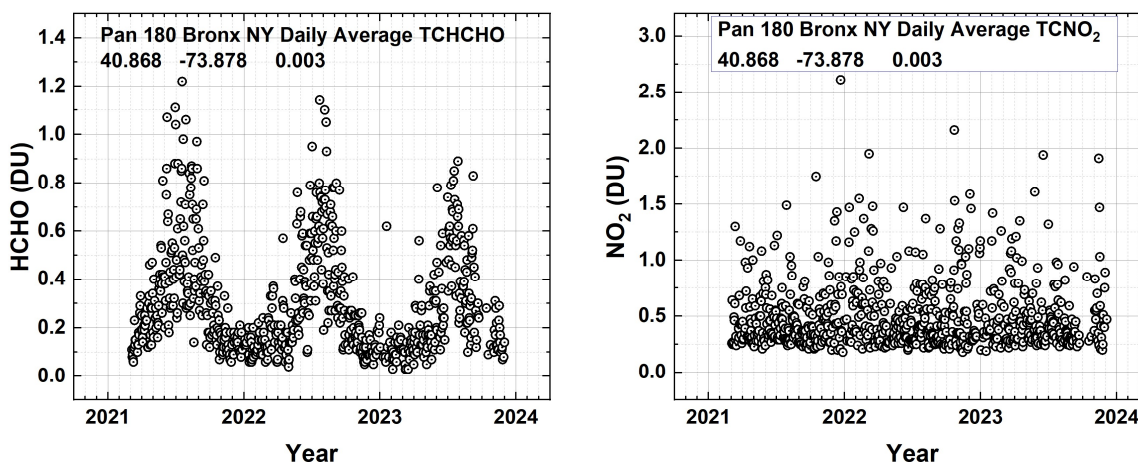182   local standard time similar to the OMI overpass time.

Fig. 02 The daily average seasonal variation of TCHCHO and TCNO2 in DU over Fordham University in Bronx, New York City from Pandora 180 at 40.868^O latitude, -73.878^O longitude, and 0.003 km altitude. Each point is a daily average of the data in Fig.1. Local principal investigator: Dr. Luke Valin.

183

184   There are 3 Pandora sites in New York City and one in nearby Bayonne, New Jersey. The NYC sites are in
185   the Bronx-Fordham University, Manhattan-City College NY (CCNY), Queens-Queens College. All four
186   successfully measured NO_2 in the period 2021 − 2023. A strong seasonal cycle in TCNO2 is not seen (Figs.
187   1 and 2) in the traffic driven production of NO_2.in the Bronx, New York. The mean values of total column

188 NO$_2$ (TCNO2) for each of the 3 New York sites are 0.5 DU while the TCNO2 for the port city of Bayonne,
189 NJ is substantially higher at 0.7 DU. None of the four sites show a large seasonal daily average TCNO2
190 pattern. For TCHCHO, all four sites show an annual seasonal cycle with three of the sites having a 3-year
191 average of 0.3 DU except for the Queens site at 0.45 DU. The Queens site may be anomalous because of
192 many missing points affecting the average.

193 Similar behavior is seen at other sites such as the one from New Haven Connecticut located in a
194 vegetated area adjacent to two rivers (Fig.3). TCHCHO has a clear summer peak in June – July and a
195 weak winter TCNO2 peak in December to January coinciding with the maximum heating season.

196 The seasonal variation of TCHCHO could not be studied prior to the internal upgrade of Pandora after
197 2019 that was needed because of the release of HCHO from polyoxymethylene (POM-H Delrin) out-
198 gassing as a function of daytime temperature within the Pandora sun-pointing optical head (Spinei et al.,
199 2021)

200
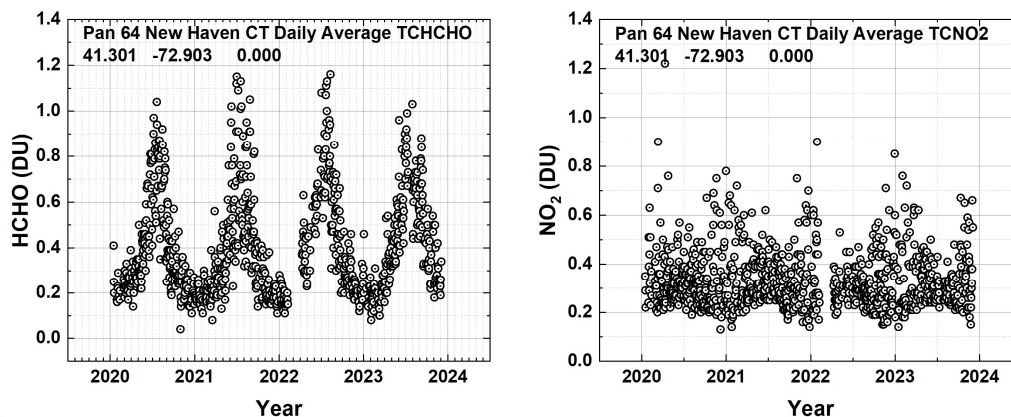
Fig. 03 The seasonal variation of TCHCHO and TCNO2 over New Haven Connecticut from Pandora 64 at
41.301^{O}N latitude and -72.903^{O}W longitude. Each point is a daily average. Local principal investigator:
Dr. Nader Abuhassan

201

202 An equatorial Pandora site (Fig. 4) with a sufficiently long data record is located in Bangkok, Indonesia
203 near a small park and lake. Bangkok has a tropical monsoon climate with three main seasons: hot season
204 from March to June, rainy season from July to October, and cool season between November and
205 February. TCHCHO has a seasonal cycle peaking in March – April when the sun is nearly overhead and a
206 minimum during the rainy season. TCNO2 has a clear seasonal cycle peaking in December – January and
207 a minimum during the rainy season. Bangkok has a tropical climate with April as the hottest month with
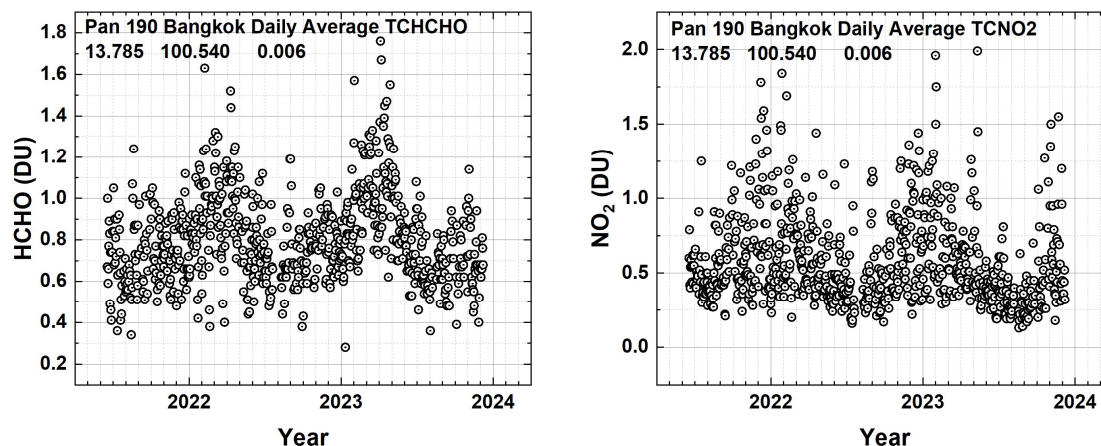208 temperatures averaging at 30.5 °C (87°F) and the coldest is December at 26 °C (79°F).

Fig. 04 The seasonal variation of TCHCHO and TCNO2 over equatorial Bangkok Indonesia at 13.785^{O}N and 100.540^{O}E. The local principal investigator is Surassawadee Phoompanit.

209

210 An unusual counter example to the typical TCHCHO seasonal cycle is for the Pandora site located in Tel
211 Aviv Israel. Tel Aviv has significant amounts of HCHO but does not show seasonal variation in TCHCHO
212 because of a coastal location in a warm climate even at midlatitudes located at 32.113^{O}N, 34.085^{O}E that
213 has essentially two seasons, a cool, rainy winter: October – April and a dry, hot summer: May –
214 September. The result is there is a limited seasonal increase in vegetational activity and almost no
215 seasonal variation in HCHO (Fig. 5). However, TCNO2 shows a clear seasonal increase in the December -
216 January months frequently reaching over 0.5DU. The TCNO2 seasonality is similar to that of the near-
217 surface concentrations reported by Boersma et al., (2009). The Pandora instrument 182 is located at Tel
218 Aviv University about 1 km from a major highway. Tel Aviv has frequent episodes of smog associated
219 with heavy automobile and truck traffic (Newmark, 2001). Heating and cooling in Tel Aviv are mainly
220 electrical with the maximum power generation occurring in the summer, suggesting that the winter
221 TCNO2 peak is not caused just by electrical power generation from natural gas that emits NO$_2$.
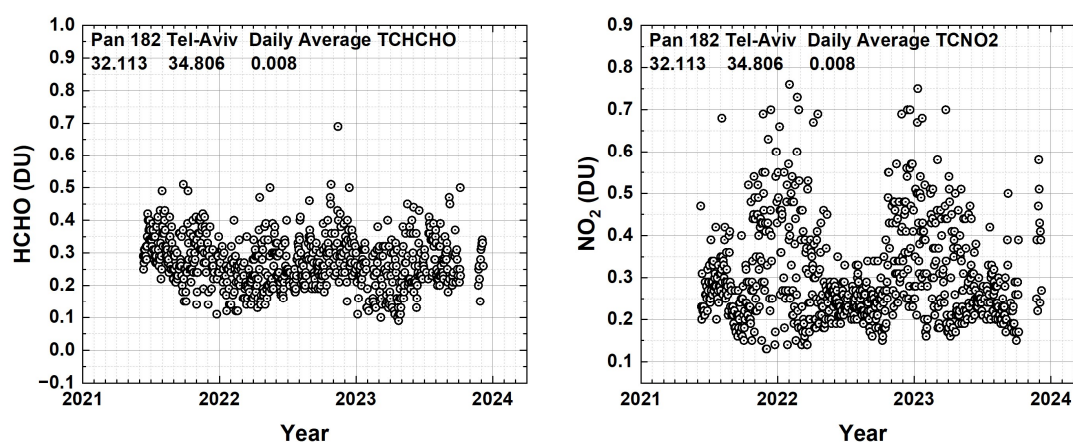
Fig. 05 Seasonal variation in daily average TCHCHO and TCNO2 in Tel Aviv Israel from Pandora 182 located at 32.113^{O}N, 34.085^{O}E at a height of 8 meters. The local principal investigator for Pan 182 is Dr. Michal Rozenhaimer.

222

223 Finally, a Pandora example from the Southern Hemisphere SH from Wakkerstroom, South Africa located
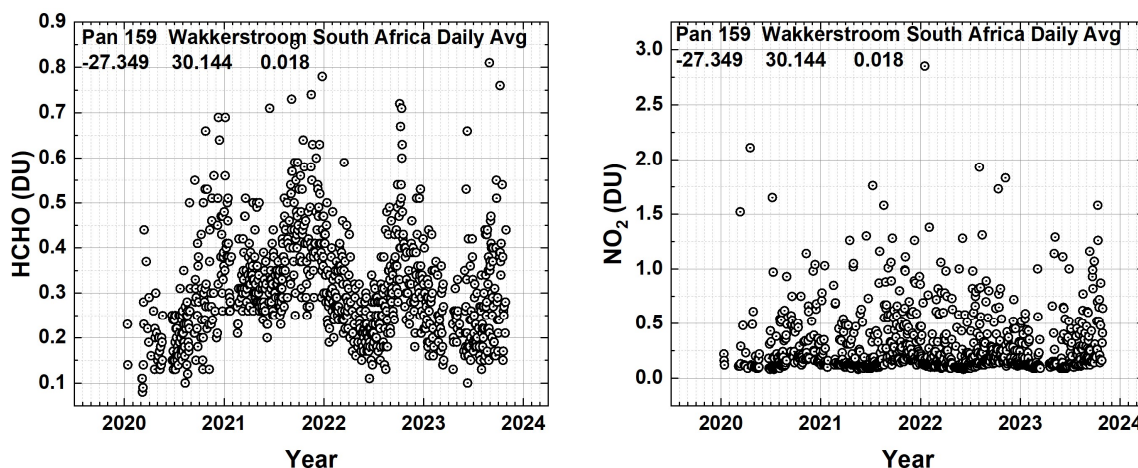224 in a rural area near the ocean a few degrees outside of the equatorial zone at -27.359^{O}S and 30.144^{O}E.

Fig. 06 Seasonal variation in daily average HCHO and NO$_2$ in Wakkerstroom South Africa from Pandora 159 located at -27.359^{O}S and 30.144^{O}E at a height of 18 m. Local principal investigator: B. Scholes

225

226 As expected, the peak value of TCHCHO occurs near the SH summer in November – December, while
227 TCNO2 has no significant seasonal dependence.

2.1 Comparisons Between Pandora and OMI Retrievals of NO$_2$ and HCHO

229 In this section three types of comparisons of Pandora with OMI satellite data are considered. First (Fig. 7
230 upper panels), is the TCNO2 time series consisting of the data record of Pandora and OMI from 2020 –
231 2023. The second (Fig. 7 lower panels) is a low-pass Lowess(3-months) filter of midday TCNO2 showing
232 the seasonal variation. The third (Fig. 8), looks at a few selected days in May, July, and December and
233 compares typical Pandora clear-sky values with the mid-afternoon OMI overpass at times near 13:30
234 hours equator crossing time. Pandora and OMI data are matched at the same GMT and then converted
235 to local solar time, GMT + Longitude/15. The OMI overpass HCHO, NO$_2$ and O$_3$ data, 2004 – 2025, are
236 found at https://zenodo.org/uploads/15468213 in 7Zip ASCII format.

237 Figure 7 (upper 2 panels) illustrates that OMI only captures the mid-day fraction of the daily values of
238 total column NO$_2$ and fails to detect the extent of the daily pollution at both the Bronx New York City
239 and Busan Korea sites. This is because OMI and other polar orbiting satellites only collect data once per
240 day (occasionally twice per day) at any given location at mid-afternoon, frequently when TCNO2 is
241 below its daily maximum (Lamsal et al., 2015; Herman et al., 2019). The lower 4 panels of Fig. 7 reveal
242 the seasonal dependence of TCNO2 at two mid-latitude Northern Hemisphere sites found by using a 3-
243 month low-pass filter Lowess(3 Months) showing that there is an annual TCNO2 cycle peaking in the
244 winter that corresponds to the natural gas and oil heating use. The Pandora (13:00 to 14:00) values are
245 larger than those from OMI especially at Busan suggesting that the OMI gridded overpass field of view
246 0.25^O x 0.25^O includes areas of lower NO$_2$ values over the nearby ocean. In the case of the Bronx, the
247 differences are smaller but also include areas over rivers. Philadelphia Pennsylvania is landlocked but
248 smaller than an OMI gridded footprint so that the OMI field of view contains somewhat less polluted
249 suburbs making the OMI TCNO2 closer to the Pandora values. The Boulder Colorado Pandora is in a

250   small landlocked city where the OMI field of view extends over sparsely populated regions leading to
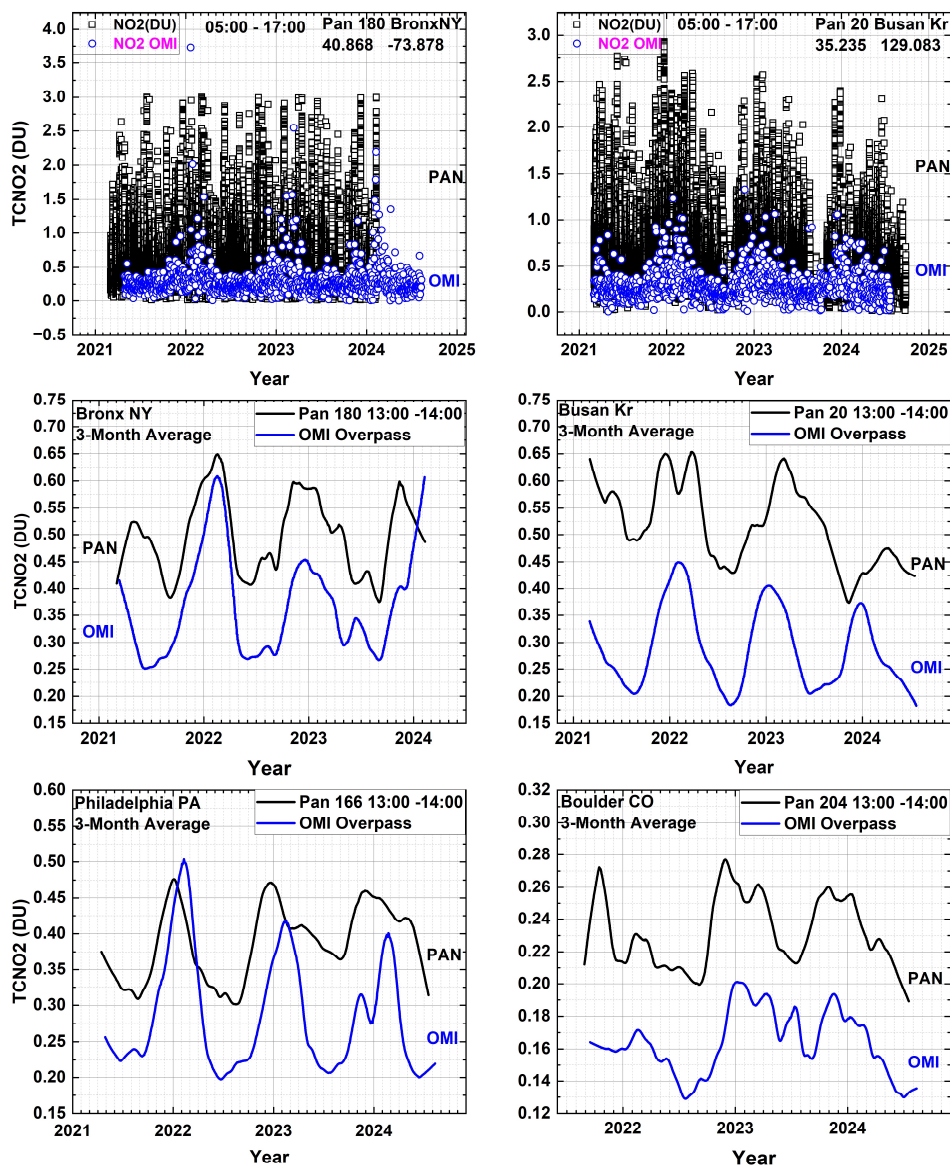
251   OMI TCNO2 lower than Pandora values.

252

Fig. 07 Upper 2 Panels: Comparison of OMI (approximately 13:30) and Pandora (07:00 – 17:00) total column NO_2 time series in Bronx NY (40.868^{O}N, -73.878^{O}W) and Busan Korea (35.235^{O}N, 129.083^{O}E). Lower 4 Panels: Pandora data for Bronx, Busan, Philadelphia (39.992^{O}N, -75.081^{O}W) and Boulder (40.0375^{O}N, -105.242^{O}W) are averaged between 13:00 – 14:00 hours. Both OMI (blue) and Pandora (black) then have a Lowess(3-month) low-pass filter applied. Local principal investigator for Pan20 is Jae Hwan Kim, for Pan 180 and Pan 166 is Dr. Luke Valin, and for Pan 204 Dr. Nader Abuhassan.

253   Figures 8 and 9 show the diurnal daytime variation for 3 selected days for Pandora retrieved total

254   column NO_2 and HCHO compared with OMI at the overpass time for both the Bronx in New York City

255   Busan, Korea and Philadelphia, Pennsylvania. These are typical examples of the highly variable hourly
256   variation of TCHCHO and TCNO2 as observed by Pandora on clear-sky days at most sites.
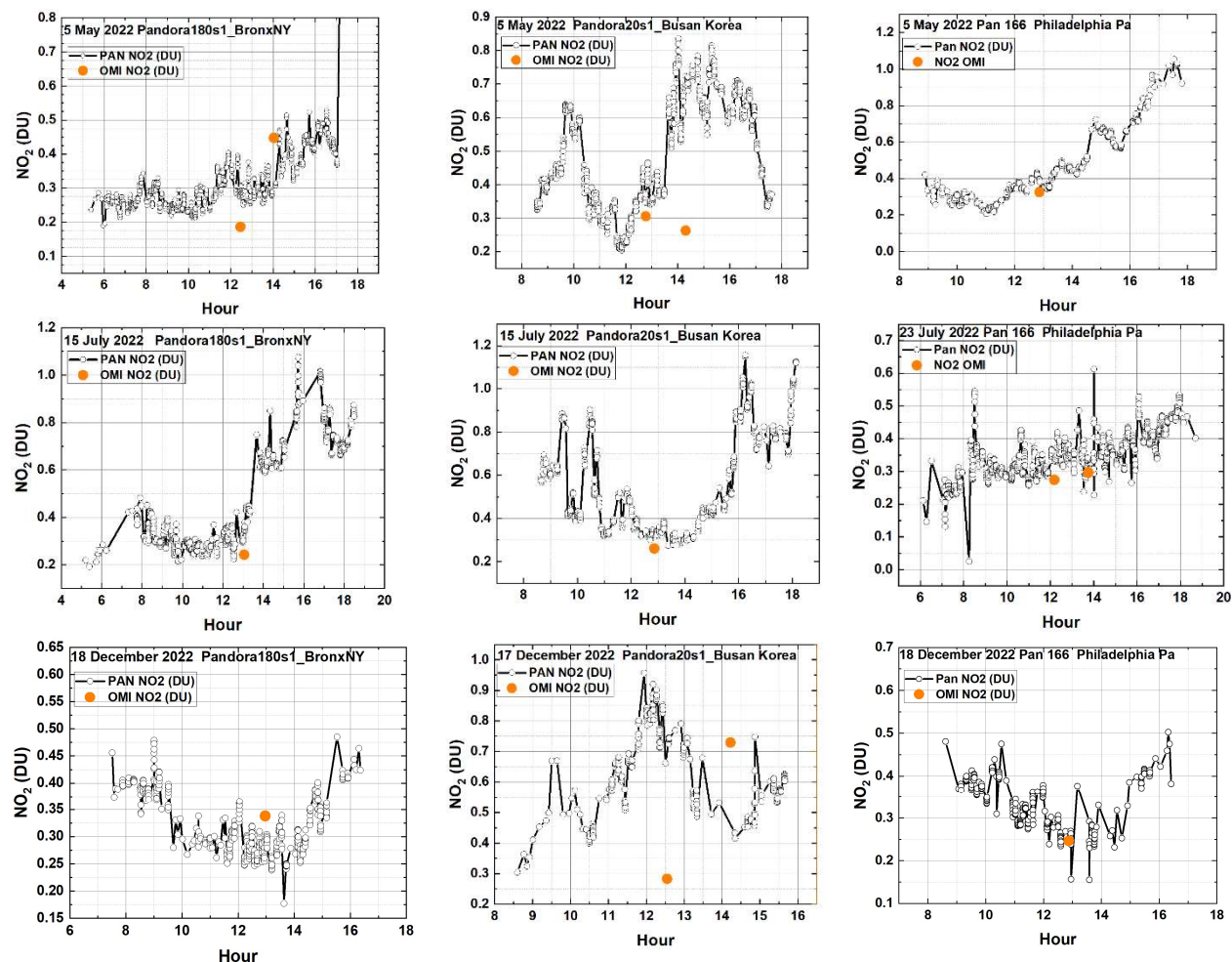
257

Fig. 08 A comparison between Pandora and OMI (Orange circle) total column NO$_2$ for 3 locations (Bronx, New York, Busan Korea, Philadelphia, Pennsylvania. The Local principal investigator for Pan 180 and Pan 166 is Dr. Lukas Valin and for Pan 20 is Dr. Jae Hwan Kim.

258

259   The hourly variation of TCHCHO and TCNO2 on any given day can take on unique shapes depending on
260   the presence of surface winds, changes in temperature, and the amount of sunlight. The variability of
261   TCNO2 is also driven by the strength of the sources (automobile exhaust, power generation, industry,
262   etc.) as well as the meteorological conditions. On some days, there is good agreement (within 10%) but
263   in general the OMI overpass values do not agree with Pandora retrieved values for both TCHCHO and
264   TCNO2. In the sample shown in Figures 8 and 9, the cases of agreement are about 70% of the time for
265   TCNO2 and 30% for TCHCHO. Also, the OMI TCNO2 frequently is less than the daily maximum of TCNO2.
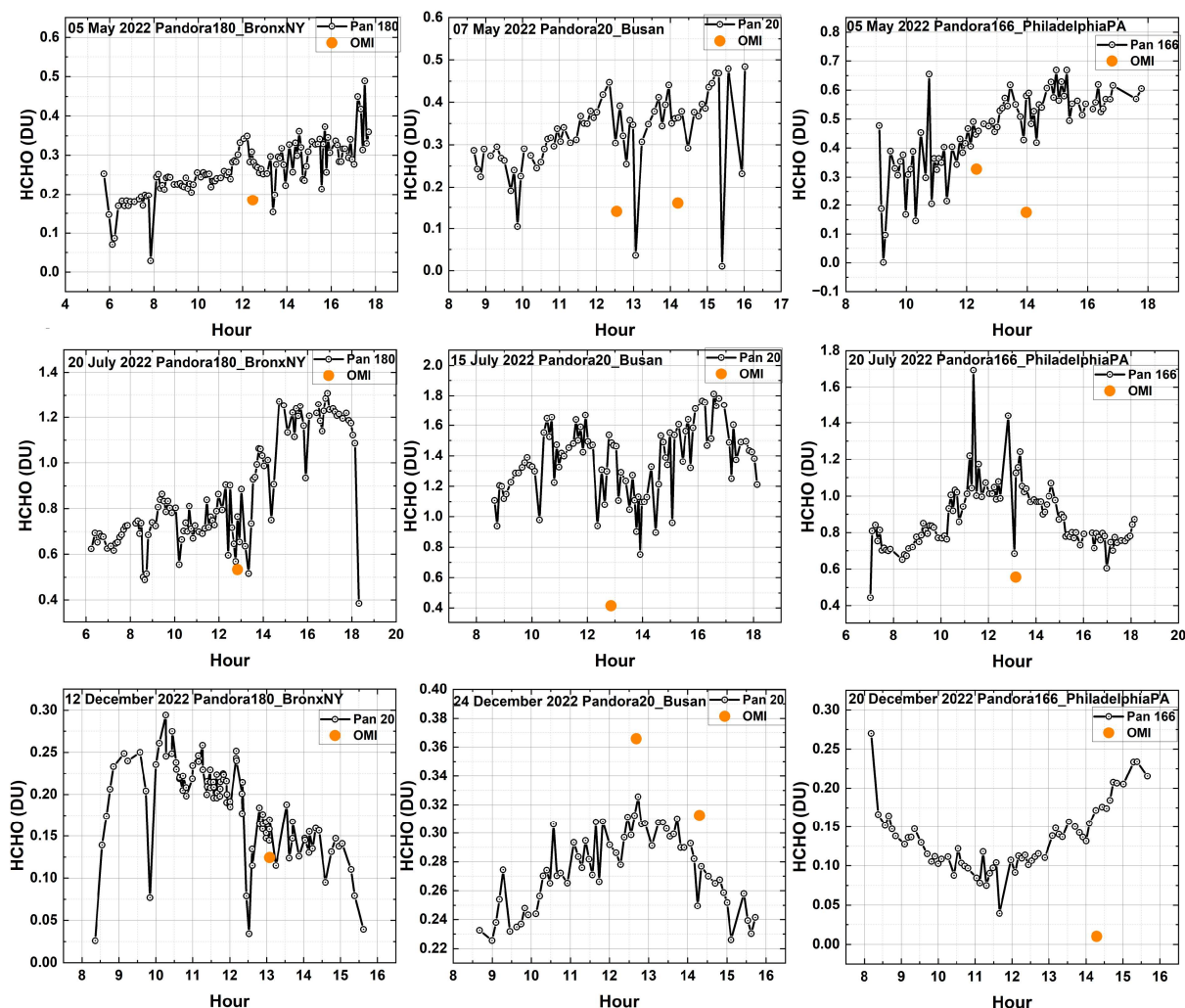
266

Fig. 09 A comparison between Pandora and OMI (orange circle) total column HCHO. The Local principal investigator for Pan 180 and Pan 166 is Dr. Luke Valin and for Pan 20 is Dr. Jae Hwan Kim.

267

268 Figure 9 illustrates the comparison of TCHCHO retrievals from Pandora and OMI. The spectral fitting
269 algorithm for detecting HCHO absorption is in the same short wavelength UV spectral region as used for
270 ozone retrieval, 300 – 360 nm (Gratien et al. 2007). This means that the retrieval sensitivity for "seeing"
271 all the way to the surface is reduced because of ozone absorption and Rayleigh scattering. Also, small
272 errors in ozone retrieval can affect the detection of HCHO. This problem is not present for the spectral
273 fitting of NO_2, since that usually occurs in the visible range 410 – 450 nm where there is only
274 interference from a weak and narrow water vapor line.

275 Pandora TCHCHO daily average data (Fig. 10) for University of Toronto in Toronto-Scarborough (Lat =
276 43.784^{O}N, Lon = -79.187^{O}W) shows clear peaks in the summer from the vegetation in a surrounding park
277 area whereas TCNO2 shows only small seasonal variation with small peaks also occurring in the summer
278 for values less than 0.4 DU. Higher values do not show any seasonal variation. The University of Toronto
279 is located near a major highway, which is a strong source of NO_2 from automobiles and trucks. Unlike
280 many sites, OMI TCHCHO data over Toronto East (centered on 43.74^{0}N, -79.27^{0}E is about 8 km from the

281   Pandora site) also shows sporadic summer peak values that are higher than the Pandora 13:00-14:00
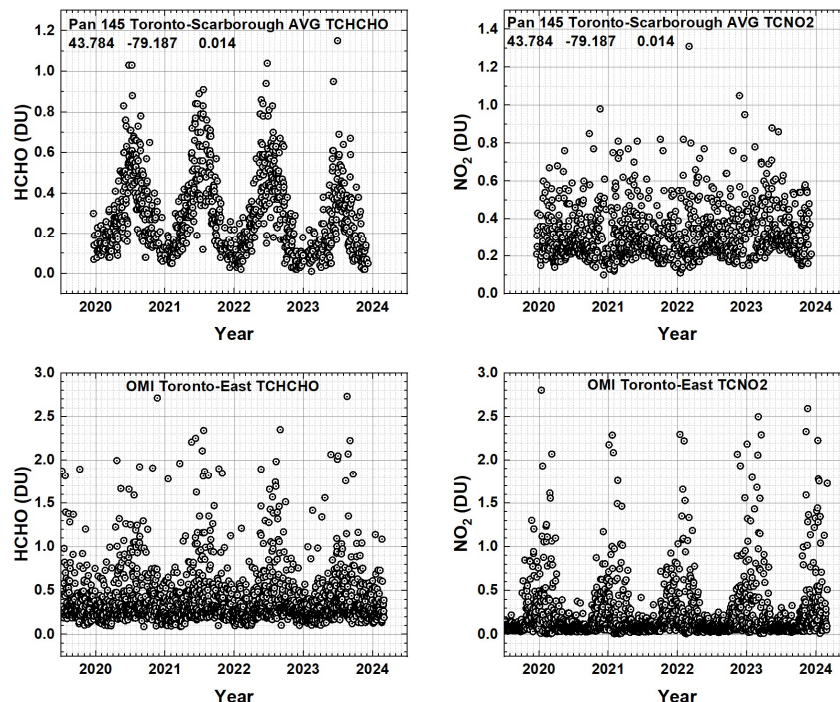282   averages and all of the Pandora data (Fig. 11).

Fig. 10 A comparison of Pandora TCHCHO and TCNO2 daily average total column amounts for Toronto-Scarborough University of Toronto and OMI data for Toronto East (43.740^{O}N, -79.270^{O}W at approximately 13:20±0:20 Local Sun Time, GMT + Longitude/15). The local principal investigator for Pan 145 is Dr. Vitali Fioletov.

283

284   Using the daily average Pandora data over Toronto-Scarborough (Fig. 10 upper right) shows no visible
285   hint of an TCNO2 annual cycle that peaks in winter while the OMI TCNO2 amounts at 13:40 show a clear
286   peak in December – January corresponding to the peak winter heating for the city (Figs. 10 lower right).
287   Instead of the daily average data, using the average TCNO2 from 13:00 to 14:00 to correspond to the
288   OMI overpass time and then applying a Lowess(3 month) low-pass filter (Fig. 11) shows less TCNO2 and a
289   weaker annual cycle that corresponds to the annual cycle observed by OMI. The OMI FOV includes the
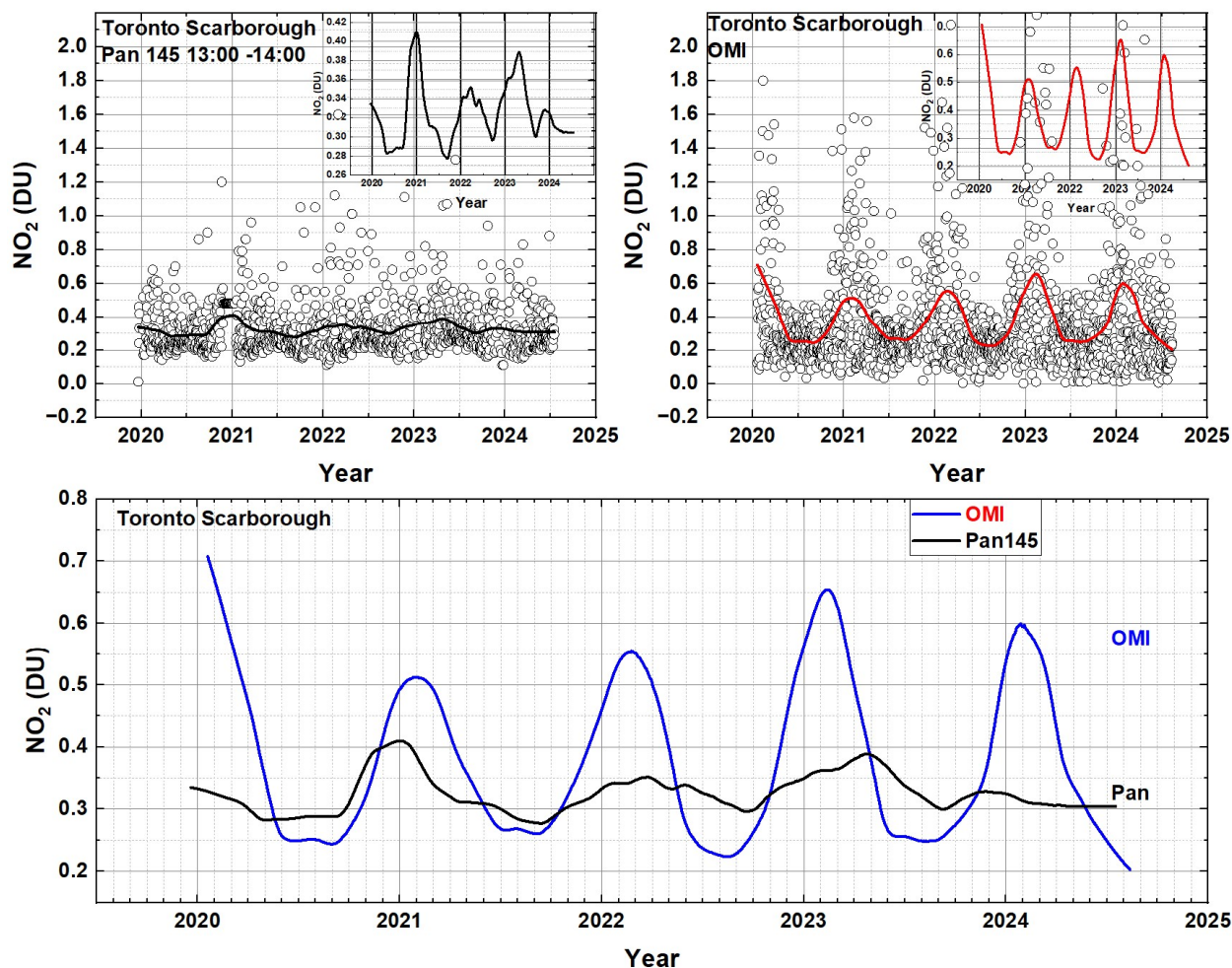290   city of Toronto.

Fig. 11 TCNO2 annual cycle for Toronto Scarborough from Pan 145 average between 13:00 and 14:00 and OMI. The smooth curves are Lowess(6 Months).

291

292 The lower panel in Fig. 11 reproduces the inset values showing the OMI has a stronger TCNO2 annual
293 cycle because it includes the city area of Toronto. Pandora 145 picks up a small amount of the seasonal
294 signal from Toronto.

295 As shown in Fig. 12, the TCHCHO low-pass filtered time series (2021 – 2024), Lowess(3-months),
296 measured by OMI and Pandora frequently do not agree. An example is the comparison over Bronx, NY
297 (Lat = 40.868^O Lon = -73.878^O) where the Pandora 180 is located in a park with a small lake, while OMI
298 gridded data is averaged over a large area 33 x 33 km^2 in New York City with little vegetation. In 5 of the
299 6 sites shown in Fig.12, the OMI retrieval shows more TCHCHO than observed by Pandora. Tsukuba,
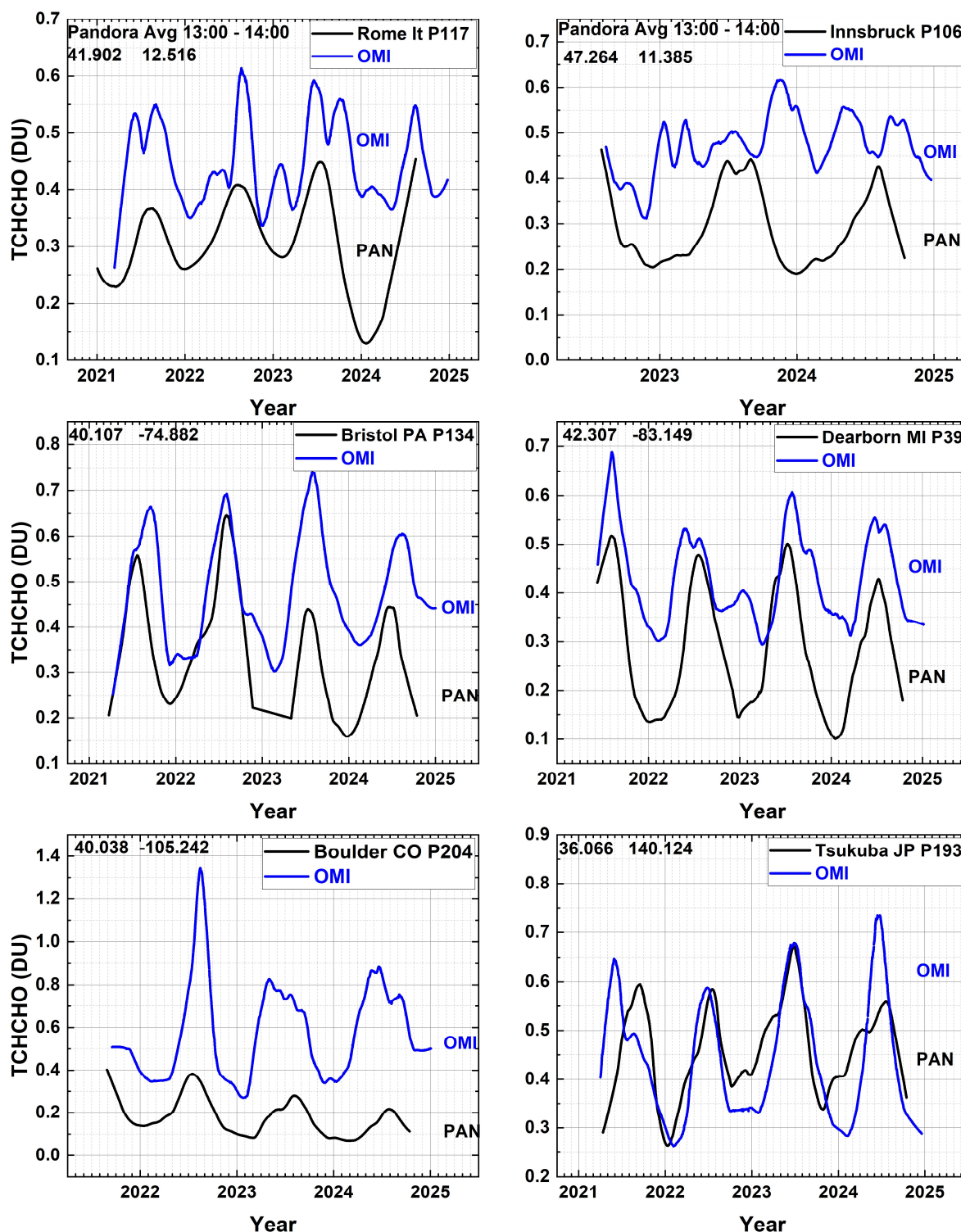300 Japan is an exception. Six additional sites are shown in the Appendix Fig. A2.

Fig. 12 A comparison between low-pass filtered, Lowess(3 months), OMI and Pandora at six sites with varying degrees of agreement with TCHCHO(Pan) < TCHCHO(OMI). The Local Principal Investigators are P106 Dr. Stefano Casadio, Dr. Kei Shiomi P193, Dr. Alexander Cede P204, Dr. Lukas Valin P39; P134, and Dr. Martin Tiefengraber P106. Latitudes and longitudes are in each upper left corner.

301

302 The disagreement over Boulder Colorado may be caused by OMI's large field of view that includes lower
303 altitude grasslands. Similarly, the Innsbruck Pandora is located in a valley at the University of Innsbruck
304 surrounded by mountain areas where TCHCHO varies over the OMI FOV. Except for a few cases (e.g.,
305 Bronx, NY and Innsbruck, Austria) OMI and Pandora see the same TCHCHO annual cycle.

2.2 Total Ozone Column

307 The retrieval of total column ozone amounts TCO (Figs. 13) serves as a check on the calibration of both
308 OMI and Pandora that is also needed for spectrally overlapping TCHCHO retrievals. Comparisons of
309 Pandora TCO with TCO measured by OMI show good agreement suggesting both instruments are well
310 calibrated in the UV range also needed for retrieving TCHCHO. The good TCO agreement is partly
311 because most of the O_3 is in the stratosphere near 25 km and the fact that ozone is slowly changing
312 spatially over the OMI field of regard for the overpass data. Figure 13 shows an example obtained over
313 Washington DC from the roof of the NASA Headquarters building and from the roof of a building at
314 Pusan University, Korea. The other sites in Table 1 show similar good monthly average agreement.
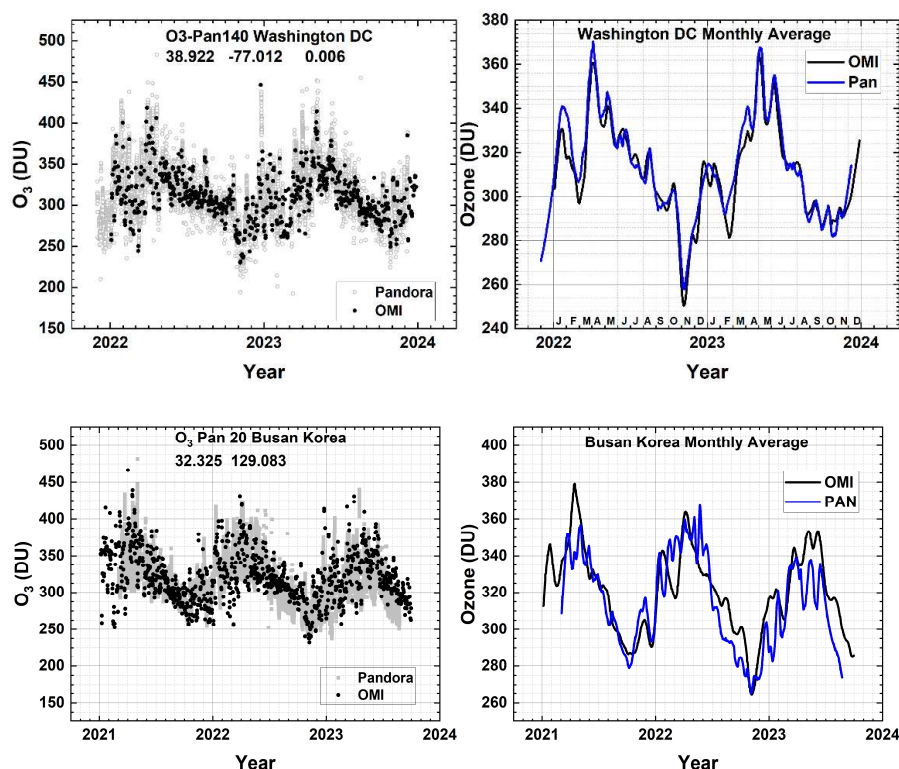
315

Fig. 13 A comparison of OMI Total Column Ozone values with those obtained from Pandora 140 over the Washington DC site at 38.922^{O}N and -77.012^{O}W and with those obtained from Pandora 20 over the Busan, Korea site at 32.325^{O}N and 129.083^{O}E. The smooth curves (right panel) are Lowess(6-month) fits to data in the left panel. The local principal investigator for Pan 140 is Dr. Jim Szykman and for Pan20 is Jae Hwan Kim.

316

317

318   A test of Pandora UV data is a comparison between EPIC, OMI and Pandora TCO at the specific OMI and
319   EPIC overpass times (Fig. 14 and 15). that shows good agreement within 1 to 3 %. OMI TCO overpass
320   data for all Pandora sites and more are available from
321   https://avdc.gsfc.nasa.gov/pub/data/satellite/Aura/OMI/V03/L2OVP/OMTO3/

322   There is also good agreement between daily OMI TCO with that obtained from Pandora (Fig. 14) at most
323   sites. The values obtained at Granada differ by about 8 DU or 2.9 %.
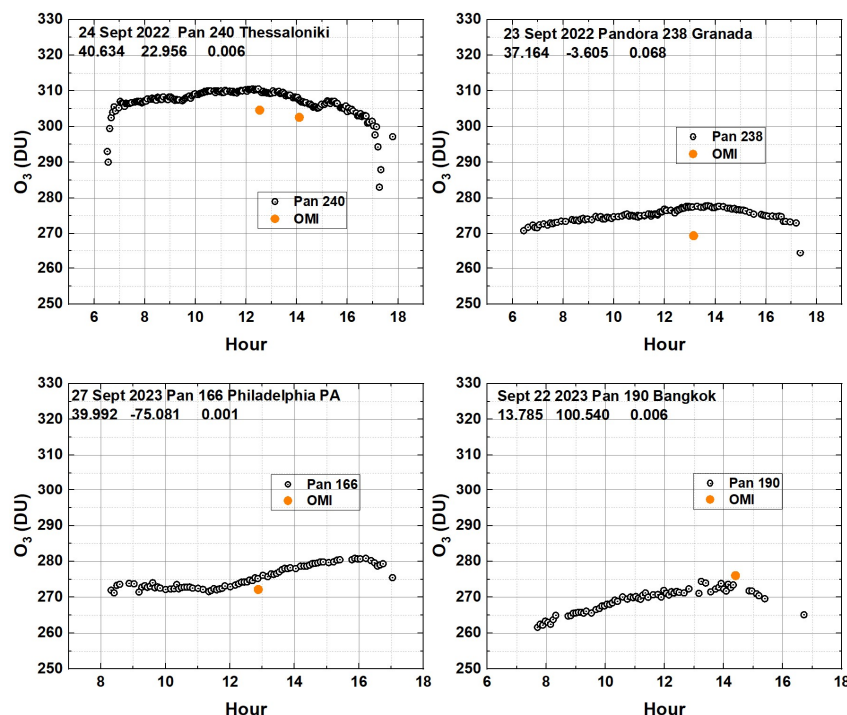
Fig. 14 A comparison of Pandora and OMI retrievals of total column O_3 at the time of the OMI satellite overpass. Local Principal Investigators: Pan 240 Alexander Cede, Pan 238 Inmaculada Foyo Moreno, Pan 166 Lukas Valin, and Pan 190 Surassawadee Phoompan.

The diurnal variation of TCO seen by Pandora can be compared (Fig. 15) with that observed by the Earth Polychromatic Imaging Camera (EPIC) on the DSCOVR (Deep Space Climate Observatory) satellite orbiting about the Earth-Sun gravitational balance Lagrange-1 point (Herman et al., 2018). EPIC obtains simultaneous data from sunrise to sunset once per hour (once per 90 minutes during Northern Hemisphere winter) as the Earth rotates in EPIC's FOV (field of view). Examples of EPIC's view of the whole illuminated Earth are available from https://epic.gsfc.nasa.gov/. The spatial resolution for TCO is 18 x 18 km^2 at the center of the image (the color images have 10 x 10 km^2 resolution). Retrievals earlier than 07:00 and after 17:00 are not reliable for EPIC or Pandora because of high solar zenith angle effects (spherical geometry effects for SZA > 75°) not included in the retrieval algorithms. In the case of EPIC, this is compounded by high View Zenith Angles VZA outside of 07:00 to 17:00 local sun time.
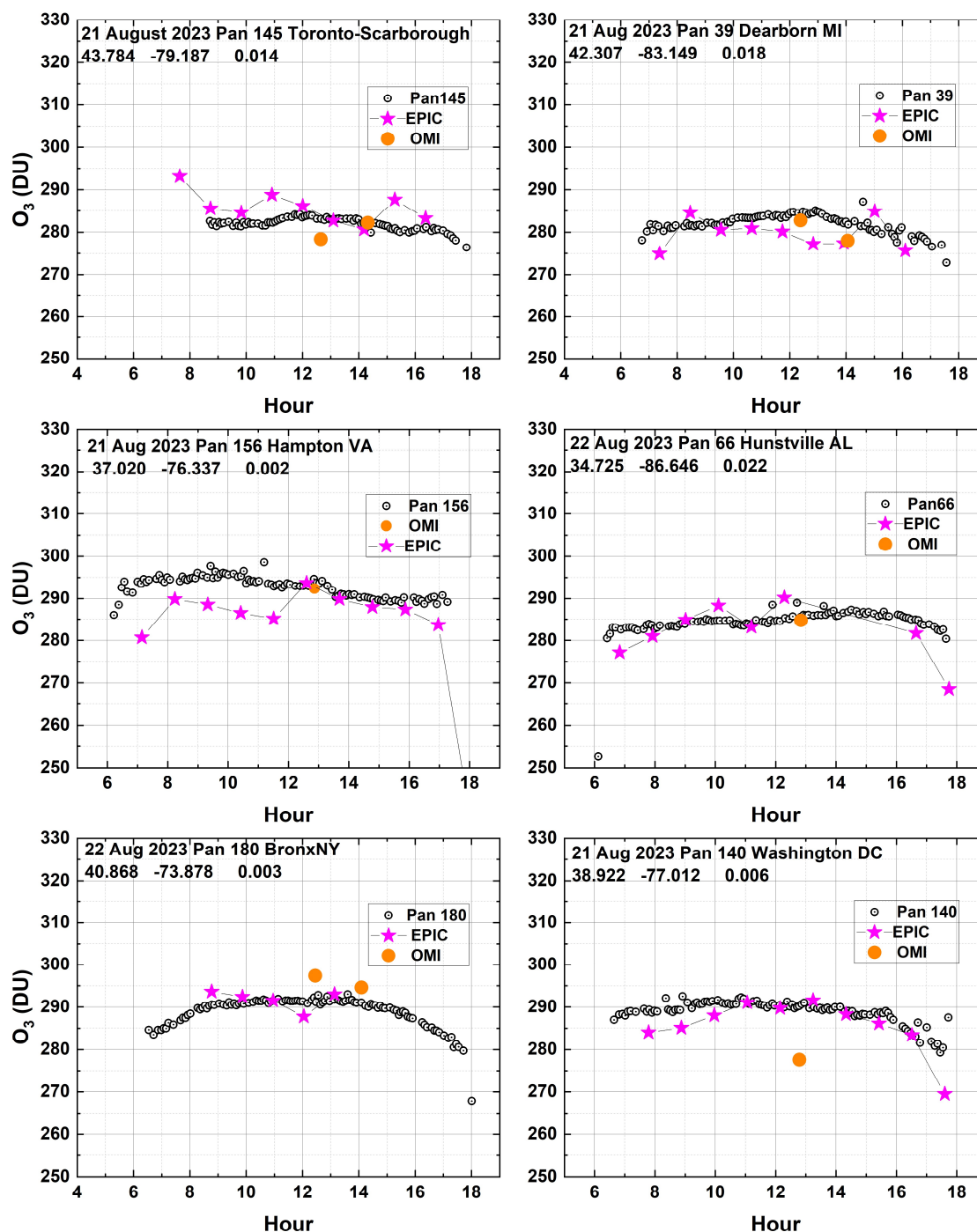
Fig. 15 A comparison of Pandora (Open Circles), EPIC (magenta stars), and OMI (orange circles) retrievals of total column O_3 at the times of the satellite overpasses. Latitude, longitude, and altitude (km) are in the upper left corner. Local Principal Investigators: Pan 145 Vitali Fioletov, Pan 66 Lukas Valin, Pan 39 Lukas Valin, Pan 156 Alexander Cede, Pan 66 Nader Abuhassan, Pan180 Lukas Valin, and Pan 140 Jim Szykman

325 For the cases shown, the TCO data are properly retrieved between 07:00 and 17:00 local solar time. The
326 10:20 and 11:30 EPIC value for Hampton, VA of 286.5 and 285DU differs from Pandora by -3 %. Other
327 differences are smaller. Occasionally, OMI differs from Pandora values as is the case, -4.6 %, for 21
328 August 2023 over Washington, DC.

329 **3.0 Summary**

330 Typical examples of the seasonal variability of HCHO, NO_2, and O_3 in terms of their measured total
331 column TCHCHO, TCNO2, and TCO have been presented from both ground-based Pandora Spectrometer
332 instruments and the OMI satellite spectrometer instrument overpass retrievals for selected Pandora
333 sites. For most sites, OMI observes the strong seasonal variation of TCHCHO that is also clearly seen in
334 the Pandora data and in surface measurements (Wang et al., 2022). OMI TCHCHO retrievals are usually
335 larger than those retrieved by Pandora but not always (Fig. A2). The amount of seasonal variation for
336 TCHCHO varies depending on the site. For most midlatitude sites, the seasonal variation is significant
337 with peak values occurring during the summer.

338

339 A comparison between the multi-year time series of Pandora and OMI TCNO2 in urban areas shows that
340 OMI is underestimating the degree of atmospheric NO_2 pollution. The results for TCNO2 and TCO agree
341 with Pandora data, 2012 – 2017, from a previous study before the Pandora upgrade (Herman et al.,
342 2019). When Pandora is limited to an average of data obtained between 13:00 and 14:00 hours, the
343 agreement between Pandora and OMI TCNO2 is better but with OMI TCNO2 frequently less than
344 observed by Pandora. Comparisons of Pandora daily diurnal time series of TCHCHO and TCNO2 with
345 OMI overpass values show agreement about 30% and 50 % of the time, respectively with OMI frequently
346 retrieving more TCHCHO than Pandora.

347 OMI TCNO2 at one shown site, Toronto-Scarborough, shows seasonal variability that the Pandora 145
348 does not appear to see. However, limiting the data to the OMI overpass time between 13:00 and 14:00
349 and applying a Lowess(3-months) low-pass filter reveals a weak annual cycle compared to OMI. This
350 could be because OMI detects the NO_2 source from winter heating in the city, while the Pandora site
351 (University of Toronto campus) is fairly remote from Toronto city buildings and is mostly affected by road
352 traffic as the source of NO_2. The same low-pass filter technique applied to other sites (e.g., Bronx, NY,
353 Busan, Korea, Philadelphia, Pennsylvania, and Boulder, Colorado) also show an annual cycle
354 corresponding to winter heating based on combustion.

355 Total column ozone agrees well in both seasonal variation and in comparison with Pandora at the OMI
356 overpass time. Given the nature of the ozone retrieval algorithm, the good agreement with TCO suggests
357 that the UV calibrations for the Pandoras and OMI are correct. At most well-calibrated Pandora sites,
358 there is good agreement between Pandora TCO with the hourly TCO obtained from the DSCOVR-EPIC
359 instrument observing the Earth from an orbit about the Earth-Sun gravitational balance Lagrange-1
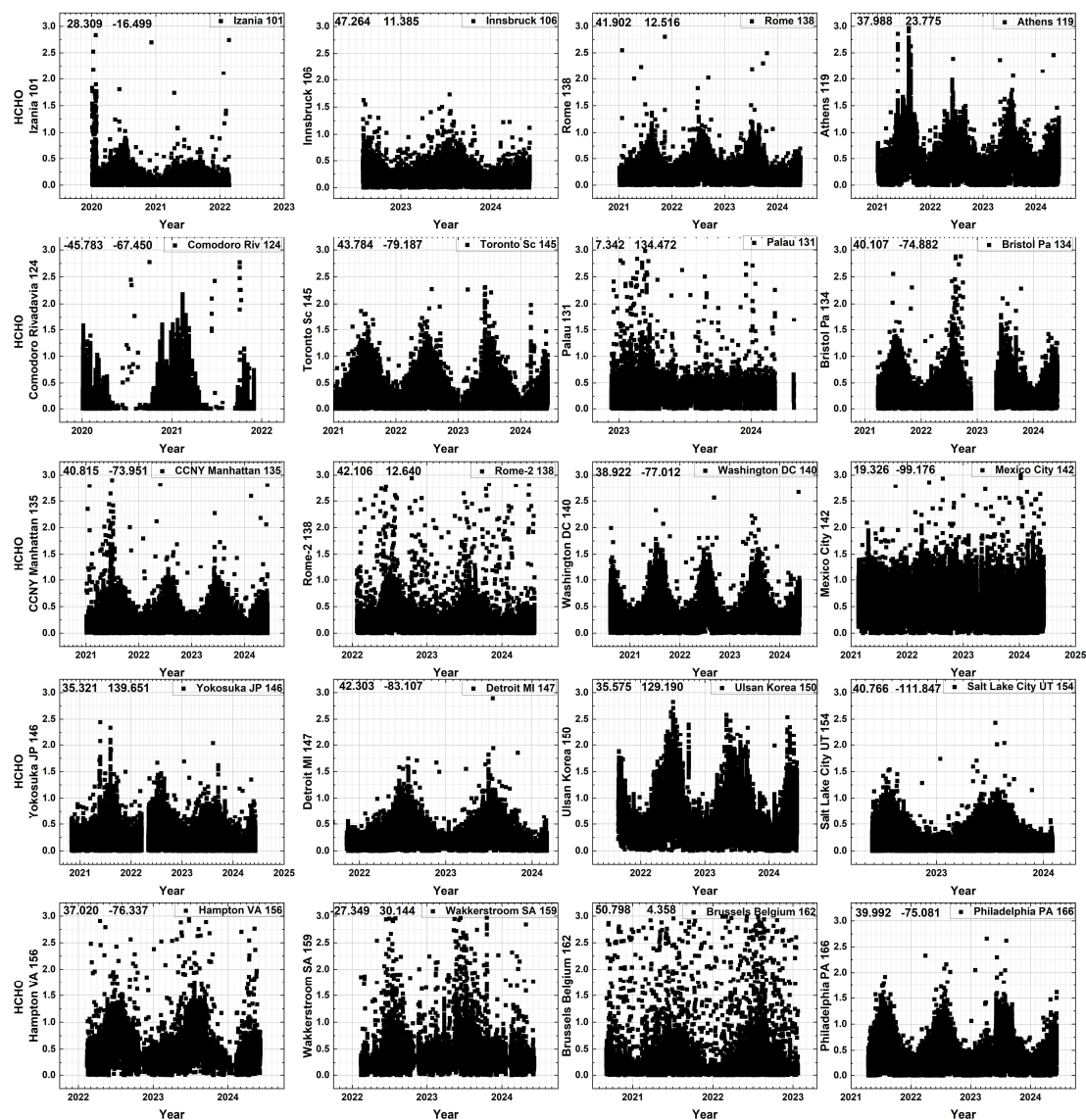360 point.

361

362

363

364

365 **Appendix**

Fig. A1 The seasonal cycle of TCHCHO in DU from 20 randomly selected Pandora TCHCHO time series. The numbers in the upper left corner are the latitude and longitude in degrees and the Pandora instrument number in the right corner.

366

367 Figure A1 shows the seasonal dependence of TCHCHO with the majority of sites showing a maximum
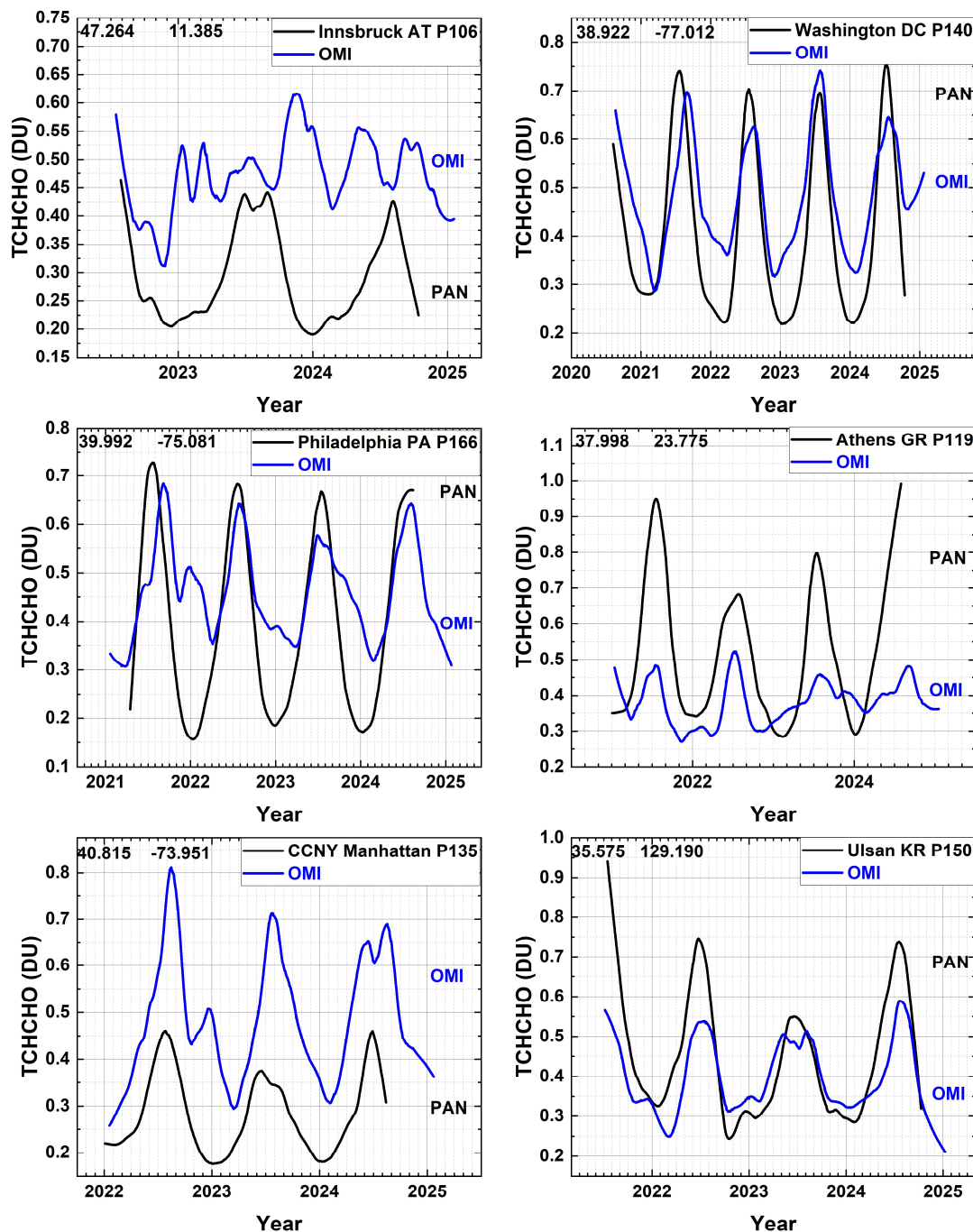368 TCHCHO in mid-summer.

Figure A2 Six cases from Fig. A1 that have significant seasonal variation in TCHCHO. The numbers in the upper left corner are the latitude and longitude in degrees and the Pandora instrument number in the right corner. Principal Investigators are: P106 Dr. Martin Tiefengraber, P140 Dr. Jim Szykman, P166 Dr. Lucas Valin, P119 Dr. Stelios Kazadsi, P135, Dr. Maria Tzortziou, and P150 Dr. Chang Keun Song.

369

370 Figure A2 shows additional cases where OMI and Pandora see the same seasonal dependence but differ
371 on the amount of TCHCHO retrieved.

4.0 References

Boeke NL, Marshall JD, Alvarez S, Chance KV, Fried A, Kurosu TP, Rappenglück B, Richter D, Walega J, Weibring P, Millet DB. Formaldehyde columns from the Ozone Monitoring Instrument: Urban versus background levels and evaluation using aircraft data and a global model, J. Geophys. Res. 2011 Mar 16;116(D5):10.1029/2010jd014870, doi: 10.1029/2010jd014870, 2011.

Boersma, Klaas & Jacob, D. & Trainic, Miri & Rudich, Yinon & De Smedt, Isabelle & R, Dirksen & Eskes, Henk, Validation of urban NO2 concentrations and their diurnal and seasonal variations observed from space (SCIAMACHY and OMI sensors) using in situ measurements in Israeli cities. Atmos Chem Phys, 9. 10.5194/acp-9-3867-2009, 2009.

Celarier, E. A., E. J. Brinksma, J. F. Gleason, J. P. Veefkind, A. Cede, J. R. Herman, D. Ionov, F. Goutail, J.-P. Pommereau, J.-C. Lambert, M. van Roozendael, G. Pinardi, F. Wittrock, A. Schönhardt, A. Richter, O. W. Ibrahim, T. Wagner, B. Bojkov, G. Mount, E. Spinei, C. M. Chen, T. J. Pongetti, S. P. Sander, E. J. Bucsela, M. O. Wenig, D. P. J. Swart, H. Volten, M. Kroon, P. F. Levelt, Validation of Ozone Monitoring Instrument nitrogen dioxide columns, Validation of Ozone Monitoring Instrument nitrogen dioxide columns, J. Geophys. Res., 113,D15S15, doi:10.1029/2007JD008908, 2008.

Cleveland, W. S.: Robust Locally Weighted Regression and Smoothing Scatterplots, J. Am. Stat. Assoc., 74, 829–836, https://doi.org/10.2307/2286407 , 1979.

Cleveland, W. S. and Devlin, S. J.: Locally Weighted Regression: An Approach to Regression Analysis by Local Fitting, J. Am. Stat. Assoc., 83, 596–610, https://doi.org/10.1080/01621459.1988.10478639 , 1988.

De Smedt, I., Pinardi, G., Vigouroux, C., Compernolle, S., Bais, A., Benavent, N., Boersma, F., Chan, K.-L., Donner, S., Eichmann, K.-U., Hedelt, P., Hendrick, F., Irie, H., Kumar, V., Lambert, J.-C., Langerock, B., Lerot, C., Liu, C., Loyola, D., Piters, A., Richter, A., Rivera Cárdenas, C., Romahn, F., Ryan, R. G., Sinha, V., Theys, N., Vlietinck, J., Wagner, T., Wang, T., Yu, H., and Van Roozendael, M.: Comparative assessment of TROPOMI and OMI formaldehyde observations and validation against MAX-DOAS network column measurements, Atmos. Chem. Phys., 21, 12561–12593, https://doi.org/10.5194/acp-21-12561-2021 , 2021.

Faustini, Annunziata and Rapp, Regula and Forastiere, Francesco, Nitrogen dioxide and mortality: review and meta-analysis of long-term studies, European Respiratory Journal,44, 744-753, https://doi.org/10.1183/09031936.00114713 , 2014.

Fu, W., Zhu, L., Kwon, A., Park, R. J., Lee, G. T., Smedt, I. D., Liu, S., Li, X., Chen, Y., Pu, D., Li, J., Zuo, X., Zhang, P., Li, Y., Yan, Z., Zhang, X., Zhang, J., Wu, X., Shen, H., . . . Yang, X., Evaluating GEMS HCHO Retrievals With TROPOMI Product, Pandora Observations, and GEOS-Chem Simulations. Earth and Space Science, 12(1), e2024EA003894. https://doi.org/10.1029/2024EA003894 , 2025.

Gratien, A., B. Picquet-Varrault , J. Orphal , E. Perraudin , J.-F. Doussin and J.-M. Flaud , Laboratory intercomparison of the formaldehyde absorption cross sections in the infrared (1660–1820 cm^{-1} and ultraviolet (300–360 nm) spectral regions, *J. Geophys. Res.*, **112** , https://doi.org/10.1029/2006JD007201, D05305 1-10, 2007.

418   Herman, J., A. Cede, E. Spinei, G. Mount, M. Tzortziou, and N. Abuhassan, NO$_2$ column amounts from
419   ground-based Pandora and MFDOAS spectrometers using the direct-sun DOAS technique:
420   Intercomparisons and application to OMI validation, *J. Geophys. Res.*, 114, D13307,
421   doi:10.1029/2009JD011848, 2009.

423   Herman, J., Huang, L., McPeters, R., Ziemke, J., Cede, A., and Blank, K.: Synoptic ozone, cloud reflectivity,
424   and erythemal irradiance from sunrise to sunset for the whole earth as viewed by the DSCOVR
425   spacecraft from the earth sun Lagrange 1 orbit, Atmos. Meas. Tech., 11, 177-194,
426   https://doi.org/10.5194/amt-11-177-2018, 2018.

428   Herman, J., Abuhassan, N., Kim, J., Kim, J., Dubey, M., Raponi, M., and Tzortziou, M.: Underestimation of
429   column NO$_2$ amounts from the OMI satellite compared to diurnally varying ground-based retrievals from
430   multiple PANDORA spectrometer instruments, Atmos. Meas. Tech., 12, 5593–5612,
431   https://doi.org/10.5194/amt-12-5593-2019, 2019.

433   Judd, L. M., Al-Saadi, J. A., Janz, S. J., Kowalewski, M. G., Pierce, R. B., Szykman, J. J., Valin,
434   L. C., Swap, R., Cede, A., Mueller, M., Tiefengraber, M., Abuhassan, N., and Williams, D.:
435   Evaluating the impact of spatial resolution on tropospheric NO$_2$ column comparisons
436   within urban areas using high-resolution airborne data, Atmos. Meas. Tech., 12, 6091–
437   6111, https://doi.org/10.5194/amt-12-6091-2019 , 2019.

439   Kim, K. H., Jahan, S. A., & Lee, J. T., Exposure to Formaldehyde and Its Potential Human Health
440   Hazards. *Journal of Environmental Science and Health, Part C*, *29*(4), 277–299.
441   https://doi.org/10.1080/10590501.2011.629972, 2011.

443   Lamsal, L. N., Krotkov, N. A., Celarier, E. A., Swartz, W. H., Pickering, K. E., Bucsela, E. J., Gleason, J. F.,
444   Martin, R. V., Philip, S., Irie, H., Cede, A., Herman, J., Weinheimer, A., Szykman, J. J., and Knepp, T. N.:
445   Evaluation of OMI operational standard NO2 column retrievals using in situ and surface-based NO2
446   observations, Atmos. Chem. Phys., 14, 11587–11609, https://doi.org/10.5194/acp-14-11587-2014 ,
447   2014.

449   Lamsal, L., Duncan, Bryan, Yoshida, Yasuko, Krotkov, Nickolay, Pickering, Kenneth, Streets, David, Lu,
450   Zifeng, U.S. NO2 trends (2005–2013): EPA Air Quality System (AQS) data versus improved observations
451   from the Ozone Monitoring Instrument (OMI). Atmospheric Environment. 110.
452   10.1016/j.atmosenv.2015.03.055, 2015.

454   Levelt, P. F., Joiner, J., Tamminen, J., Veefkind, J. P., Bhartia, P. K., Stein Zweers, D. C., Duncan, B. N.,
455   Streets, D. G., Eskes, H., van der A, R., McLinden, C., Fioletov, V., Carn, S., de Laat, J., DeLand, M.,
456   Marchenko, S., McPeters, R., Ziemke, J., Fu, D., Liu, X., Pickering, K., Apituley, A., González Abad, G.,
457   Arola, A., Boersma, F., Chan Miller, C., Chance, K., de Graaf, M., Hakkarainen, J., Hassinen, S., Ialongo, I.,
458   Kleipool, Q., Krotkov, N., Li, C., Lamsal, L., Newman, P., Nowlan, C., Suleiman, R., Tilstra, L. G., Torres, O.,
459   Wang, H., and Wargan, K.: The Ozone Monitoring Instrument: overview of 14 years in space, Atmos.
460   Chem. Phys., 18, 5699–5745, https://doi.org/10.5194/acp-18-5699-2018, 2018.
461   Morfopoulos C, Müller J-F, Stavrakou T, et al. Vegetation responses to climate extremes recorded by
462   remotely sensed atmospheric formaldehyde. Glob Change Biol., 28, 1809–1822.
463   https://doi.org/10.1111/gcb.15880, 2021.
464

465 Lorente, A., Folkert Boersma, K., Yu, H., Dörner, S., Hilboll, A., Richter, A., Liu, M., Lamsal, L. N., Barkley,
466 M., De Smedt, I., Van Roozendael, M., Wang, Y., Wagner, T., Beirle, S., Lin, J.-T., Krotkov, N., Stammes, P.,
467 Wang, P., Eskes, H. J., and Krol, M.: Structural uncertainty in air mass factor calculation for NO_2 and HCHO
468 satellite retrievals, Atmos. Meas. Tech., 10, 759–782, https://doi.org/10.5194/amt-10-759-2017 , 2017.
469
470 Newmark, G. (2001). Emissions Inventory Analysis of Mobile Source Air Pollution In Tel Aviv, Israel,
471 Transportation Research Record, Vol. 1750, p. 40-48, https://doi.org/10.3141/1750-0, 2001.

472 Nussbaumer, C. M., Crowley, J. N., Schuladen, J., Williams, J., Hafermann, S., Reiffs, A., Axinte, R.,
473 Harder, H., Ernest, C., Novelli, A., Sala, K., Martinez, M., Mallik, C., Tomsche, L., Plass-Dülmer, C., Bohn,
474 B., Lelieveld, J., and Fischer, H.: Measurement report: Photochemical production and loss rates of
475 formaldehyde and ozone across Europe, Atmos. Chem. Phys., 21, 18413–18432,
476 https://doi.org/10.5194/acp-21-18413-2021 , 2021.

477 Peng, W.-X., X.-C. Yue, H.-L. Chen, N.L. Ma, Z. Quan, Q. Yu, C. Sonne, A review of plants formaldehyde
478 metabolism: Implications for hazardous emissions and phytoremediation, J. Hazard. Mater. 436 Article
479 129304, https://doi.org/10.1016/j.jhazmat.2022.129304, 2022.
480
481 Pinardi, G., Van Roozendael, M., Hendrick, F., Theys, N., Abuhassan, N., Bais, A., Boersma, F., Cede, A.,
482 Chong, J., Donner, S., Drosoglou, T., Dzhola, A., Eskes, H., Frieß, U., Granville, J., Herman, J. R., Holla, R.,
483 Hovila, J., Irie, H., Kanaya, Y., Karagkiozidis, D., Kouremeti, N., Lambert, J.-C., Ma, J., Peters, E., Piters, A.,
484 Postylyakov, O., Richter, A., Remmers, J., Takashima, H., Tiefengraber, M., Valks, P., Vlemmix, T., Wagner,
485 T., and Wittrock, F.: Validation of tropospheric NO_2 column measurements of GOME-2A and OMI using
486 MAX-DOAS and direct sun network observations, Atmos. Meas. Tech., 13, 6141–6174,
487 https://doi.org/10.5194/amt-13-6141-2020 , 2020.

488 Spinei, E., Whitehill, A., Fried, A., Tiefengraber, M., Knepp, T. N., Herndon, S., Herman, J. R., Müller, M.,
489 Abuhassan, N., Cede, A., Richter, D., Walega, J., Crawford, J., Szykman, J., Valin, L., Williams, D. J., Long,
490 R., Swap, R. J., Lee, Y., Nowak, N., and Poche, B.: The first evaluation of formaldehyde column
491 observations by improved Pandora spectrometers during the KORUS-AQ field study, Atmos. Meas. Tech.,
492 11, 4943–4961, https://doi.org/10.5194/amt-11-4943-2018 , 2018.

493 Spinei, E., Tiefengraber, M., Müller, M., Gebetsberger, M., Cede, A., Valin, L., Szykman, J., Whitehill, A.,
494 Kotsakis, A., Santos, F., Abbuhasan, N., Zhao, X., Fioletov, V., Lee, S. C., and Swap, R.: Effect of
495 polyoxymethylene (POM-H Delrin) off-gassing within the Pandora head sensor on direct-sun and multi-
496 axis formaldehyde column measurements in 2016–2019, Atmos. Meas. Tech., 14, 647–663,
497 https://doi.org/10.5194/amt-14-647-2021 , 2021.

498 Stavrakou, T., Müller, J.-F., Bauwens, M., Boersma, K. F. & van Geffen, J. Satellite evidence for changes in
499 the NO_2 weekly cycle over large cities. *Sci. Rep.* https://doi.org/10.1038/s41598-020-66891-0 (2020).

500 Tzortziou, M., Herman, J.R., Cede, A. *et al.* Spatial and temporal variability of ozone and nitrogen dioxide
501 over a major urban estuarine ecosystem. *J Atmos Chem* **72**, 287–309, https://doi.org/10.1007/s10874-
502 013-9255-8, 2015.

503 Van der A, R. J., H. J. Eskes, K. F. Boersma, T. P. C. van Noije, M. Van Roozendael, I. De Smedt, D. H. M. U.
504 Peters, and E. W. Meijer, Trends, seasonal variability and dominant NOx source derived from a ten year
505 record of NO2 measured from space, J. Geophys. Res., 113, D04302, doi:10.1029/2007JD009021, 2008.

506   Wang, P.; Holloway, T.; Bindl, M.; Harkey, M.; De Smedt, I. Ambient Formaldehyde over the United
507   States from Ground-Based (AQS) and Satellite (OMI) Observations. Remote Sens. 14, 2191,
508   https://doi.org/10.3390/rs14092191, 2022.

509   Wittrock, F., Richter, A., Oetjen,H., Burrows, Wittrock, F., Richter,A., Oetjen,H., Burrows, J.P., Kanakidou,
510   Myriokefalitakis, S.,Volkamer,R., Beirle,S.,Platt,U., and Wagner, T.: Simultaneous global observations of
511   glyoxal and formaldehyde fromspace, Geophys. Res. Lett., 33, L16804,
512   https://doi.org/10.1029/2006GL026310,2006, 2006.

513   Zhao, X., Griffin, D., Fioletov, V., McLinden, C., Davies, J., Ogyu, A., Lee, S. C., Lupu, A., Moran, M. D.,
514   Cede, A., Tiefengraber, M., and Müller, M.: Retrieval of total column and surface NO_2 from Pandora
515   zenith-sky measurements, Atmos. Chem. Phys., 19, 10619–10642, https://doi.org/10.5194/acp-19-
516   10619-2019 , 2019.

517   Zhang, Y., Li, R., Min, Q., Bo, H., Fu, Y., Wang, Y., & Gao, Z. (2019). The controlling factors of atmospheric
518   formaldehyde (HCHO) in Amazon as seen from satellite. Earth and Space Science, 6, 959–971,
519   https://doi.org/ 10.1029/2019EA000627, 2019.

520   **Author contribution**:

521   Jay Herman is responsible for writing the paper and creating the figures. Jianping Mao obtained the
522   EPIC overpass data for the Pandora sites and discussed aspects of the paper.

523   **Data Availability**
524   Worldwide Pandora data for 63 sites is available from the Austrian Pandonia project website
525   https://data.pandonia-global-network.org/ or from a NASA backup site updated every week.
526   https://avdc.gsfc.nasa.gov/pub/DSCOVR/Pandora/DATA_02/
527   The OMI overpass TCHCHO and TCNO2 data are found at
528   https://avdc.gsfc.nasa.gov/pub/data/satellite/Aura/OMI/V03/L2OVP/OMHCHO/.

529   https://avdc.gsfc.nasa.gov/pub/data/satellite/Aura/OMI/V03/L2OVP/OMNO2/

530   OMI TCO overpass data are available from
531   https://avdc.gsfc.nasa.gov/pub/data/satellite/Aura/OMI/V03/L2OVP/OMTO3/

532

533   **Competing interests**:
534   The authors declares that they have no conflicts of interest.

535

538
539   **Acknowledgements**:
546

547   **Figure Captions**

548   Fig. 1 Seasonal and daily behavior of HCHO and NO_2 from Pan 180 located in the Bronx, NYC at 40.868^ON,
549   -73.878^OW. The blue lines are a Lowess(0.033) fit to the data (light grey), which is approximately a 1-
550   month local least-squares average. The Local principal investigator for Pan 180 is Dr. Luke Valin.

551   Fig. 2 The daily average seasonal variation of HCHO and NO_2 over Fordham University in Bronx, New
552   York City from Pandora 180 at 40.868^O latitude, -73.878^O longitude, and 0.003 km altitude. Each point is
553   a daily average of the data in Fig.1. Local principal investigator: Dr. Luke Valin

554   Fig. 3 The seasonal variation of TCHCHO and TCNO2 over New Haven Connecticut from Pandora 64 at
555   41.301^ON latitude and -72.903^OW longitude. Each point is a daily average. Local principal investigator:
556   Dr. Nader Abuhassan.

557   Fig. 4 The seasonal variation of TCHCHO and TCNO2 over equatorial Bangkok Indonesia at 13.785^ON and
558   100.540^OE. The local principal investigator is Surassawadee Phoompanit.

559   Fig. 5 Seasonal variation in daily average TCHCHO and TCNO2 in Tel Aviv Israel from Pandora 182 located
560   at 32.113^ON 34.085^OE at a height of 8 meters. The local principal investigator for Pan 182 is Dr. Michal
561   Rozenhaimer.

562   Fig. 6 Seasonal variation in daily average HCHO and NO_2 in Wakkerstroom South Africa from Pandora
563   159 located at -27.359^OS and 30.144^OE. Local principal investigator: B. Scholes

564   Fig. 7 Upper 2 Panels: Comparison of OMI (approximately 13:30) and Pandora (07:00 – 17:00) total
565   column NO_2 time series in Bronx NY (40.868^ON, -73.878^OW) and Busan Korea (35.235^ON, 129.083^OE).
566   Lower 4 Panels: Pandora data for Bronx, Busan, Philadelphia (39.992^ON, -75.081^OW) and Boulder
567   (40.0375^ON, -105.242^OW) are averaged between 13:00 – 14:00 hours. Both OMI (blue) and Pandora
568   (black) then have a Lowess(3-month) low-pass filter applied. Local principal investigator for Pan20 is Jae
569   Hwan Kim, for Pan 180 and Pan 166 is Dr. Luke Valin, and for Pan 204 Dr. Nader Abuhassan.

570   Fig. 8 A comparison between Pandora and OMI (Orange circle) total column NO_2 for 3 locations (Bronx,
571   New York, Busan Korea, Philadelphia, Pennsylvania. The Local principal investigator for Pan 180 and Pan
572   166 is Dr. Lukas Valin and for Pan 20 is Dr. Jae Hwan Kim.

573   Fig. 9 A comparison between Pandora and OMI (purple circle) total column HCHO. The Local principal
574   investigator for Pan 180 is Dr. Luke Valin and for Pan 20 is Dr. Jae Hwan Kim.

575   Fig. 10 A comparison of Pandora TCHCHO and TCNO2 daily average total column amounts for Toronto-
576   Scarborough University of Toronto and OMI data for Toronto East (43.740^ON, -79.270^OW at
577   approximately 13:20±0:20 Local Sun Time, GMT + Longitude/15). The local principal investigator for Pan
578   145 is Dr. Vitali Fioletov.

579   Fig. 11 TCNO2 annual cycle for Toronto Scarborough from Pan 145 average between 13:00 and 14:00
580   and OMI. The smooth curves are Lowess(6 Months).

        Fig. 12 A comparison between low-pass filtered, Lowess(3 months), OMI and Pandora at six sites with

varying degrees of agreement with TCHCHO(Pan) < TCHCHO(OMI). The Local Principal Investigators are P106 Dr. Stefano Casadio, Dr. Kei Shiomi P193, Dr. Alexander Cede P204, Dr. Lukas Valin P39; P134, and

581 Dr. Martin Tiefengraber P106. Latitudes and longitudes are in each upper left corner.

582 Fig. 13 A comparison of OMI Total Column Ozone values with those obtained from Pandora 140 over the
583 Washington DC site at 38.922^{O}N and -77.012^{O}W and with those obtained from Pandora 20 over the
584 Busan, Korea site at 32.325^{O}N and 129.083^{O}E. The smooth curves (right panel) are Lowess(6-month) fits
585 to data in the left panel. The local principal investigator for Pan 140 is Dr. Jim Szykman and for Pan20 is
586 Jae Hwan Kim.

587 Fig. 14 A comparison of Pandora and OMI retrievals of total column O_3 at the time of the OMI satellite
588 overpass. Local Principal Investigators: Pan 240 Alexander Cede, Pan 238 Inmaculada Foyo Moreno, Pan
589 166 Lukas Valin, and Pan 190 Surassawadee Phoompan.

590 Fig. 15 A comparison of Pandora (Open Circles), EPIC (magenta stars), and OMI (orange circles) retrievals
591 of total column O_3 at the times of the satellite overpasses. Local Principal Investigators: Pan 145 Vitali
592 Fioletov, Pan 66 Lukas Valin, Pan 39 Lukas Valin, Pan 156 Alexander Cede, Pan 66 Nader Abuhassan,
593 Pan180 Lukas Valin, and Pan 140 Jim Szykman.

594 Fig. A1 The seasonal cycle of TCHCHO in DU from 20 randomly selected Pandora TCHCHO time series.
595 The numbers in the upper left corner are the latitude and longitude in degrees and the Pandora
596 instrument number in the right corner.

597 Figure A2 shows additional cases where OMI and Pandora see the same seasonal dependence but differ
598 on the amount of TCHCHO retrieved.

599

600 **Author contribution**:

601 Jay Herman is responsible for writing the paper and creating the figures. Jianping Mao obtained the
602 EPIC overpass data for the Pandora sites and discussed aspects of the paper.

603 **Data Availability**
604 Worldwide Pandora data for 63 sites is available from the Austrian Pandonia project website
605 https://data.pandonia-global-network.org/ or from a NASA backup site updated every week.
606 https://avdc.gsfc.nasa.gov/pub/DSCOVR/Pandora/DATA_02/
607 The OMI overpass TCHCHO and TCNO2 data are found at
608 https://avdc.gsfc.nasa.gov/pub/data/satellite/Aura/OMI/V03/L2OVP/OMHCHO/.

609 https://avdc.gsfc.nasa.gov/pub/data/satellite/Aura/OMI/V03/L2OVP/OMNO2/

610 OMI TCO overpass data are available from
611 https://avdc.gsfc.nasa.gov/pub/data/satellite/Aura/OMI/V03/L2OVP/OMTO3/

612

613 **Competing interests**:
614 The authors declares that they have no conflicts of interest.

615

626